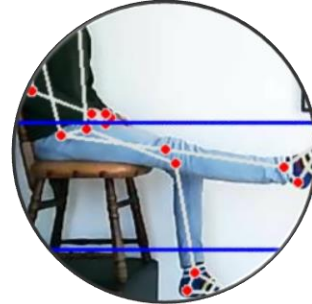
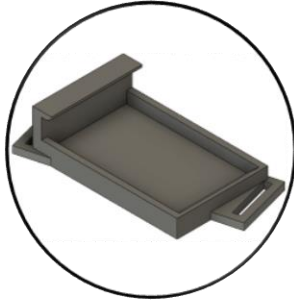


# Design of a measuring device for knee joint angle as part of a pain-relearning therapy for arthroplasty-patients



By Christopher Merkle

S4302338

Master Thesis

June 2022

supervised by Hans Timmerman and Elisabeth Wilhelm

---

# Table of contents

Report outline.....	1
Ethics paragraph.....	2
Identification of key ethical issues .....	2
Societal impact .....	2
Cost-benefit analysis .....	2
Introduction.....	3
Problem definition.....	6
Objectives.....	7
Requirements and justifications .....	7
System analysis .....	9
Justification for simplification of knee model.....	9
Methods.....	10
Concepts .....	11
<i>Discussion</i> .....	26
Results summary and concept selection.....	33
Final design .....	34
Preprocessing .....	36
<i>Classification</i> .....	39
Results.....	44
Discussion.....	47
Conclusion .....	48
References.....	48

---

# Report outline

## Guideline for the report

This project report entails an ethics chapter pointing out important ethical issues and outweighing them with their benefits, an introduction chapter describing all necessary information to understand the following parts, an objective chapter that defines what the project's aims are as well as the requirements, a methods chapter that introduces three concepts to achieve the objectives, a final design chapter that describes hardware and software of the chosen sensor system, a result chapter and a discussion chapter that puts the results into perspective involving limitations and literature fit.

Codes can be found within each corresponding folder named like the headings within the report. +

## Referencing

If a reference is located mid-sentence, it means that the leading statement is derived from the given source. If a reference is located in the end of a paragraph, it means that the leading paragraph is derived from the given source.

## Abbreviations

*Table 1 Abbreviations and their long form within the following report*

Abbreviation	Long form
IMU	Inertial measuring unit (leading "s" or "t" is shank or thigh)
RMSE	Root mean square error
CM	Compensatory movement
OA	Offset angle
TKA	Total knee arthroplasty
KNN	K nearest neighbor
SVC	Support vector machine
RFC	Random forest classifier
ROM	Range of motion
HP	Hyperparameter

## Ethics paragraph

This paragraph summarizes the identification of key ethical issues within this project, its potential societal impact and then evaluates their balance.

### Identification of key ethical issues

The project aimed to identify a healthy from a compensatory movement execution. For that, a sensor system as well as a data-collection and processing pipeline to take this decision were proposed. If it identifies squat as non-squat, it conditions the patient towards performing a wrong movement and therefore causes a decrease in rehabilitation quality. If it identifies non-squat as a squat, it again promotes compensatory movements. Alternatively, if the patient does not trust the algorithm's judgement, he/she patient would be demotivated. Thus, this project had the issue of being able to differentiate the two given categories.

Although not tackled within this thesis, the successive project team needs to consider the resolution of the visual interface to ensure full immersion of the patient. If that is not the case, it might cause the patient to experience nausea.

The inertial measuring units, the casing and straps pose a risk of skin irritation.

A very small number of participants was recruited for verification and validation. The involvement of participants again causes another ethical issue calling for a cost-benefit analysis to see if the costs of this project outweigh the benefits.

### Societal impact

Guided home training increases the immersion of rehabilitation practice. This gives the patient more quality of life since he/she can incorporate the training more freely in the day and in a more comfortable setting than in a physiotherapeutic center alone. Moreover, the quality of rehabilitation will increase through this technology since the temporal monitoring frequency increases from 1-2 per week to whatever training interval is agreed upon between the patient and physiotherapist. Further, with self-training, the responsibility for rehabilitation outcome transfers to the patient. This causes the patient to feel a higher impact of his own contribution to his problems, giving him/her access to his/her own success.

Since physiotherapist would potentially already receive feedback from the home-training, in-patient sessions with the therapist might be more efficient and problem-based. Altogether, the time for unpredictable outcomes during the rehabilitation status evaluation procedure will be less. I.e., if the home-based training gives an indication of wrong-doing in two out of ten tasks, the focus could be set onto these two tasks. This way, sessions become more predictable in their timing and waiting time for other patients could be reduced.

### Cost-benefit analysis

Since the identified issues are mild side-effects (nausea, skin irritation) and the outcome could be an increased quality of rehabilitation, added feeling of autonomy and responsibility over the patient's own rehabilitation success, it is thought that the project, is overall more beneficial. Also taking into account that all side-effects can be immediately stopped (by stop looking at the visual interface, taking the device off) and there potentially is an alternative method of rehabilitation (conservative in-patient physiotherapy), to test this project's methodology outweighs its risks. Participants are planned to be asked to participate and introduced to why their data was collected. Only after oral consent, data is going to be anonymously collected and treated confidentially.

# Introduction

This project is about monitoring the knee motion to reduce compensatory movements for total knee arthroplasty (TKA) patients. TKA is a surgery to reduce pain, restore range of motion and thereby revive quality of life for the patient population. Briefly, anatomy and the indications for a TKA are described.

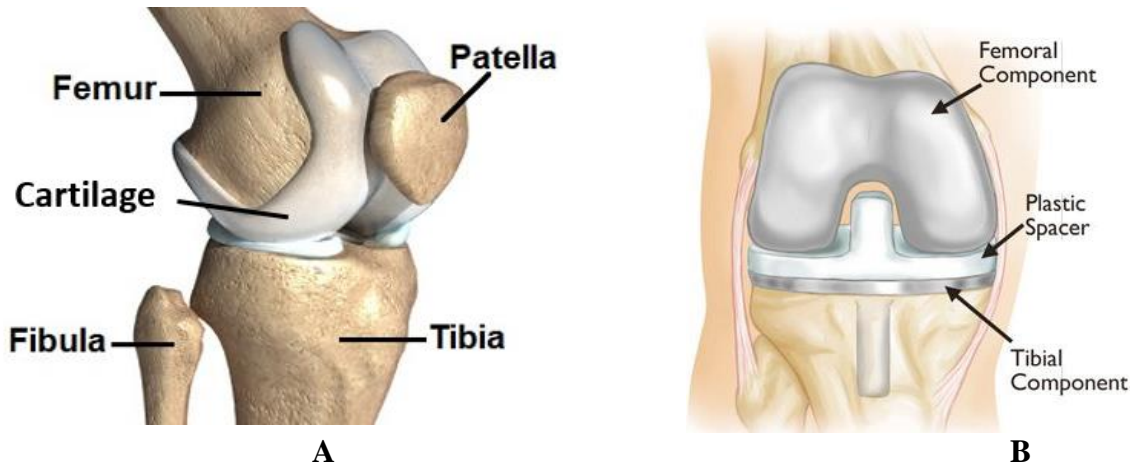


Figure 1 Bony structures and cartilage in the knee joint (A) and individual parts of total knee prosthesis (B). A modified from (1), B from (2)

The knee or tibiofemoral joint is located where the femur and tibia meet (Figure 1 - A). The patella is located anteriorly on top of the femur within the patellofemoral groove. The distal end of the femur is rounded off and rests on the tibial plateau with two bony processes called femoral condyles. Tibial condyles accompany the femoral ones on the opposite side. Articular cartilage is a white, hard, 2 to 4 mm thick connective tissue that is present whenever two bones meet to form a joint. These properties give rise to an interaction with minimal wear, optimal bone motion and shock absorption. In the knee, articular cartilage covers the distal end of the femur, the plateau of the tibia and the posterior side of the patella. (3)

Many different diseases such as osteoarthritis, rheumatoid arthritis or gout degenerate joint cartilage in fingers, shoulders, knees and feet. Degenerated cartilage gives rise to higher friction between femur and tibia which can potentially destroy the joint. (3) This can cause pain, decreased range of motion and impaired knee functionality. Non-surgical rehabilitation procedures such as physiotherapeutic programs to strengthen the neuromuscular network are successful for more than 60% of patients (4). If these non-surgical measures do not improve functionality or pain relief, a possible surgery is TKA. This procedure replaces the tibial plateau, distal femoral articular cartilage, and the femur-facing side of the patella with a titanium or cobalt-chromium prosthesis (Figure 1 - B). A polyethylene spacer is used to create a smooth surface between interfaces.

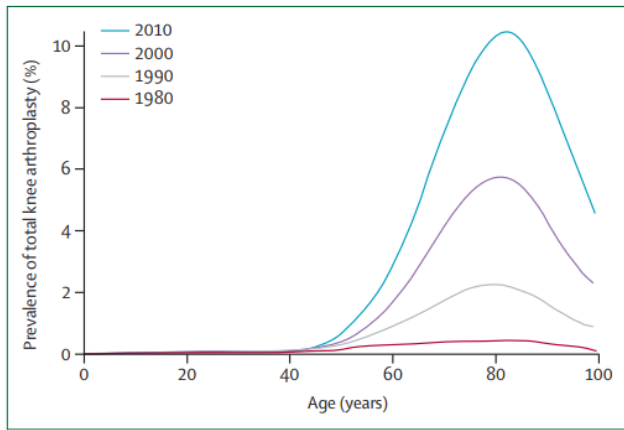


Figure 2 Prevalence of TKA-patients in total US population in percent versus age compared for different years. From (5)

In the past, TKA on obese patients or patients younger than 55 years were avoided due to the likelihood of perioperative risks and revision surgery (Figure 3) (6). However, recent studies showed that pain relief as a result of TKA is similar across the body mass index spectrum, broadening its indications (7). Moreover, no longer the surgeon but the patient ultimately decides whether to undertake surgery. Therefore, the total number of surgeries increases rapidly. In the US alone, about 600,000 patients annually undergo a TKA (5). In the Netherlands, 19,800 surgeries are done every year (8).

It was shown by a systematic review, the surgery mostly satisfies patients (4). However, due to ongoing pain, up to 20% of patients remain unsatisfied (9). In a review by Pinedo-Villanueva et. al (2018) comprising more than 100,000 patients who underwent TKA in England between 2012 and 2015, the pain is characterized mostly by night pain and limping, hence reducing the overall quality of life (9). After surgery, other disadvantageous effects are loss of the ability to control muscular activity to perform a planned movement (sensorimotor control), loss of joint stability during activity execution (functional stability) (10)(11), reduced range of motion (ROM) (12) and loss of proprioception [P]. Out of all these reasons, we can infer the socio-economic benefit of improvement in peri-operative care of TKA.

Compensatory movement (CM) patterns arise that compensate for these downsides and immediately restore function (13). CMs can also stem from habit in the late stages of any of the above-mentioned diseases (11). During gait, CMs can be increased hip external rotation (11) or decreased knee flexion (12) and are caused by decreased quadriceps force (14), decreased ham strings force (15), and decreased hip abductor force (11). It is thought that CMs have an unfavorable impact on the outcome of rehabilitation (13). Also, reducing CM aids recovery (16). It was found that these movement patterns are contributing to secondary orthopedic problems such as joint contractures and muscle reduction (13)(17). Moreover, asymmetric CMs introduce increased loading on the intact limb giving rise to a higher risk of contralateral impairment (18).

Although historically, implant design was targeted as a measure for reduction of CM, today research rather suggests improving perioperative care (5). In practice, physiotherapy is used to decrease the use of CM (19). However, entirely relying on this approach is time-consuming, expensive and has a low monitoring frequency [P]. Therefore, complementary to physiotherapy, a system that allows for guided and feedbacked home-training could potentially improve rehabilitation results.

One of the criteria to determine the success of rehabilitation is the range of motion of knee extension and flexion [P]. In healthy individuals, the passive range of motion is  $0^{\circ}$  to  $135^{\circ}$  (20). After surgery, the threshold to release the patient from stationary hospital care is  $90^{\circ}$  [P]. After the entire rehabilitation process, range of motion should be from  $0^{\circ}$  extension to  $110^{\circ}$  flexion [P]. Moreover, the occurrence of CM can be used as an indicator of rehabilitation progress [P].

Christiansen et al. (2015) conducted feedbacked home-training that complements post-TKA physiotherapy with a Wii Balance Board (Nintendo) and a series of games that entailed tasks such as bilateral-stance to lunging. Although, they found increased extension moments during gait and decreased 5-time sit-to-stand test duration, they did not focus on compensatory movement detection (21). Zeni et al. (2013) used a feedbacked home-training protocol that entailed a leg-press device that monitored the force under both feet. Moreover, they again used a Wii Balance Board to monitor between-limb weight distribution in tasks like wall-slide or squatting. By that, they tried to re-establish symmetrical movement for everyday activities. Although they focused on compensatory movement reduction by feedbacking towards symmetry, their setup required constrained foot position which excludes necessary daily activities such as walking stairs (22).

Xiao et al. (2022) utilized a 3D camera system based on Microsoft Kinect to detect and provide visual guidance to correct compensatory upper-limb movement (19). Identification of CM was done by choosing a set of movement characteristics such as shoulder lift or lateral flexion of the trunk. By utilizing the BodyFrameSource datatype, they were able to derive these parameters from Kinect data (Xbox). They successfully proved that the system could improve rehabilitation effects. In a pilot study, Cai et. Al (2019) let seated patients perform upper-limb tasks while recording pressure data from a mat mounted onto the chair (23). Support-vector machine (a machine-learning algorithm) was successfully used on the dataset to categorize different compensatory movements. A study by Borges et. al, 2012 used inertial data from stroke patients to obtain quantitative insights for upper-limb compensatory movements in different tasks such as reaching (24). Placement repeatability was insured by choosing five bony processes. They implied that other sensor locations might also be used.

## Problem definition

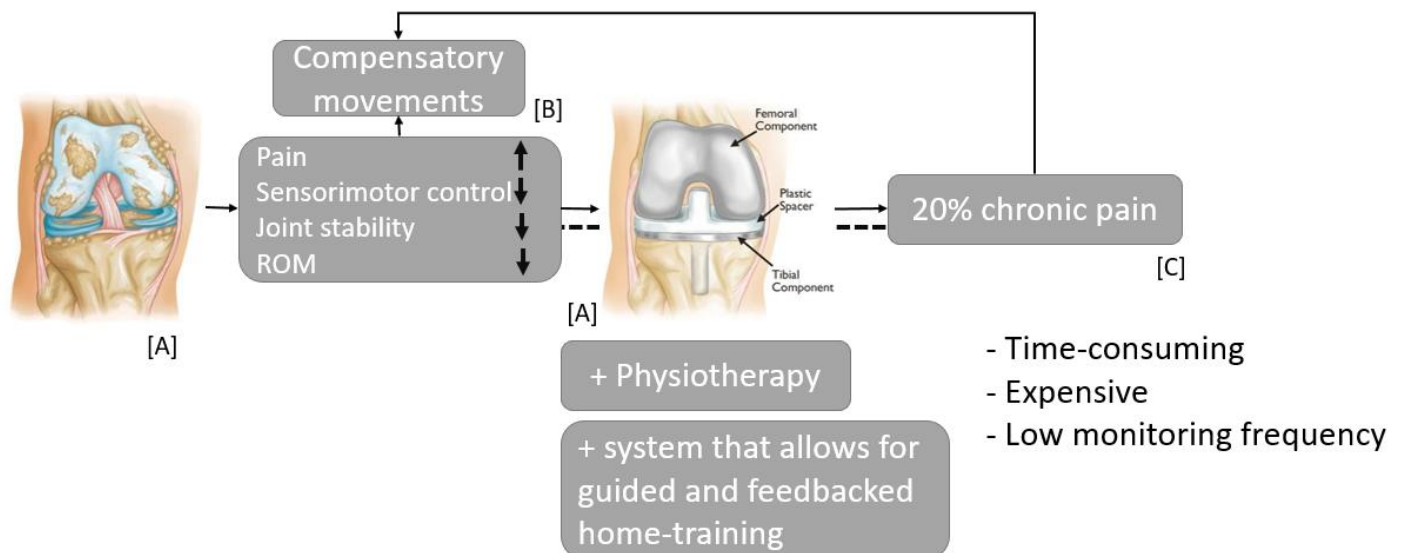


Figure 3 Schematic of problem definition starting with a diseased knee and ending in a demand for a feedbacked home-training. Arrows between boxes indicate how one item leads to another while the dashed line indicates how some downsides might still prevail. Arrows inside the boxes indicate “increased” or “decreased” depending on their orientation. With A from (2), B from (25) and C from (26)

When any cartilage degenerating disease causes pain, reduction in sensory motor control, joint stability, or range of motion, CMs develop (Figure 3). TKA is a possible surgery to re-establish full functionality and control. However, even after surgery, downsides might prevail including all the previously mentioned and scar tissue, skin irritations and cuts, again leading to CMs. To counteract, physiotherapy is added post-TKA. Since physiotherapy has its own disadvantages of being expensive, time-consuming, and having a low monitoring frequency, an additional system that adds guidance and feedback to home-therapy might improve rehabilitation results.

To the best knowledge of the author, there is no feedbacked home-training system specifically designed to detect and monitor post-TKA patients for compensatory movements of the lower-limb. Therefore, this project will focus on the first stage of such a system: choosing a sensor that could monitor knee angle and creating an algorithm that can differentiate different movement patterns (for more detail see Objectives). In a future scope, these inputs could be used in a serious gaming environment that increases motivation and immersion.



Figure 4 Illustration of squatting exercise. From (27)

The task chosen for this project is the squat (Figure 4), a simple but effective high-demand movement frequently used in post-TKA physiotherapy. It is a closed-chain task which is defined by the fact that the foot is placed on the floor permanently, hence the knee angle changes majorly due to thigh movement.



# Objectives

This project intends to aid in the development of a system for compensatory movement detection in arthroplasty patients using sensors and has the following two objectives.

1. Design a system that can acquire knee angle.
2. Detect compensatory movements for the squat task (> 70% accuracy).

This project will focus on the acquisition and conversion of data into knee angle and a parameter that indicates compensatory movement. It will focus on the squat task as a proof of concept of the selected system after which a second thesis might take it to other tasks.

# Requirements and justifications

To determine which sensor is the best to use, I start by establishing requirements according to literature, educated guessing and talks with physiotherapists, lab technicians and my supervisor. The accumulated list of requirements is followed by a list of wishes (Table 2). If necessary, individual items are explained in further detail below.

Table 2 Requirements and wishes for a device that can acquire knee angle and detect compensatory movements for TKA-patients

Requirements
The system shall be able to acquire knee angle with a spatial resolution of less than 10° and a temporal resolution of less than 50 ms (20 Hz sampling frequency).
The detectable range of motion for knee extension and flexion shall be between -10° and 150°.
The mass of the sensor shall be limited to 500g.
The system shall be able to distinguish a squat from a CM-squat.
Wishes
The workspace within which knee motion needs to be measured shall be a 1x1x2.6m space.
Setting up the device shall not demand for an extensive preparation (set-up > 3 min) or reclothing.
The system shall be able to detect internal / external hip-rotation or shank rotation.
The system shall save the data for retrospective inspection.
The system shall be able to differentiate between thigh and shank movement (relativity of output).
The system can quantify compensatory movements.

Spatial resolution shall be less than a reading from a goniometer [P]. According to literature, goniometers can be as accurate as 10° in knee angle estimation (28).

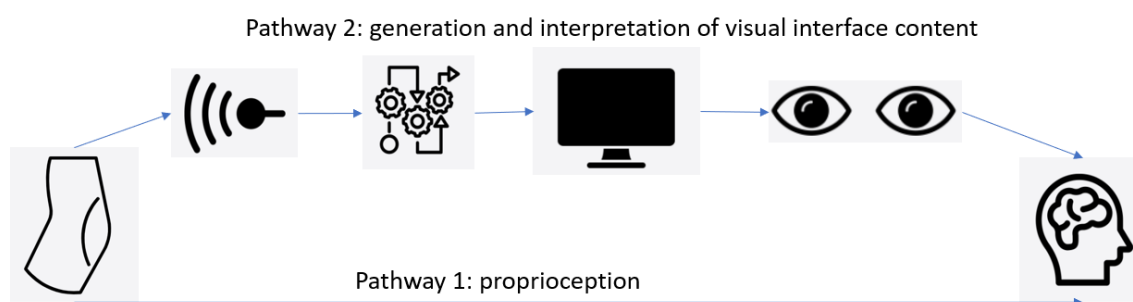


Figure 5 Proprioceptive and sensor-derived pathway from knee to brain. The sensor-derived pathway entails a sensing, processing and displaying unit.

As mentioned earlier, since this project might be used within a bigger framework that entails a serious gaming environment (Figure 5), the overall aim is to be at least equally as fast as the proprioceptive pathway from knee to brain. A paper by Stauffert et al. (2020) focusing on latency that causes cyber-sickness, suggests 50 ms to be necessary to have a responsive feeling (29).

Since passive, healthy knee extension and flexion ranges from  $0^{\circ}$  to  $135^{\circ}$  (20), some additional buffer is applied to the flexion range to account for extreme values / anatomies. Moreover, a  $-10^{\circ}$  extension range into an anatomically unrealistic state is added to allow for the detection of calibration or attachment errors. This could mean that any below-zero value indicates a faulty setup.

If the device is heavy enough to change the gait pattern within training, it will not train the patient for a real-life situation. The patient will over-actuate their knee in everyday life. To quantify this mass, a study showed that biomechanical changes due to wearable mass situated on lower limb are negligible for up to 1% of body mass (30). Considering most adult weights to be above 50kg, the mass of the device (if any) shall be limited to 500g.

To be able to monitor all training exercises, a certain area shall be monitorable. Interviewing two physiotherapists, they both stressed the fact that therapy does not always require the same area and is highly dependent on the patient [P]. If the patient lives in a three-story building without elevator, a set of two stairs is enough. If the patient is a full-time athlete, this will not be enough. However, as a minimal requirement,  $1 \times 1 \times 2.6\text{m}$  was determined.

The duration of onsite physiotherapeutic sessions varies depending on the type of rehabilitation schedule that was decided upon; they range between 20 and 60 minutes [P]. For the recommended bidaily home-training session, session duration is rather 10 to 15 min. The setup time needs to be sufficiently short to not interfere with the procedure. Interviews with therapists suggested a time window of maximally 3 minutes [P].

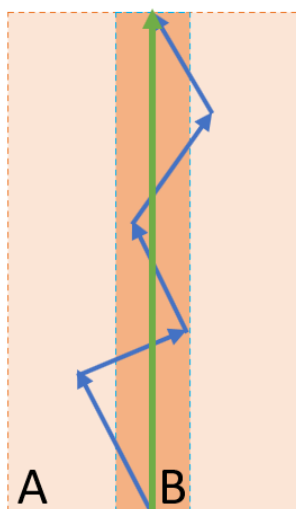


Figure 6 Quantifying compensatory movements. The green line determines the movement that should be performed, the blue line determines the patient's path. The letters A and B indicate the thresholds upon which a correction prompt is triggered.

If a patient is asked to perform a task, most likely he/she will not be able to perfectly replicate the task. If we were to correct every movement, it will be highly discouraging to continue training. Therefore, depending on the skill level, the threshold upon which a corrective message is prompted must be changed. As indicated in Figure 6 by the letters, while in skill level A, the patient's execution is considered enough, skill level B would trigger a correction prompt.

# System analysis

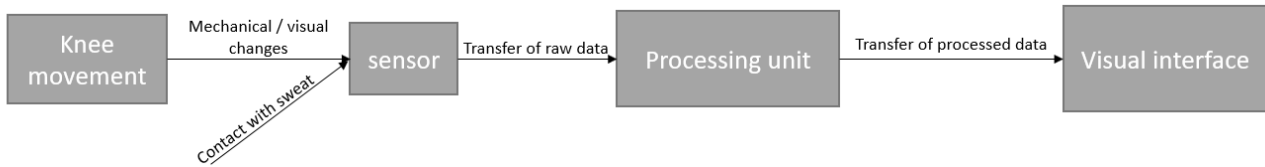


Figure 7 System analysis showing different subparts and their inputs and outputs

Knee movement will change the visual or mechanical inputs to the sensor. The sensor will create an electrical readout and transfers this to the processing unit. This will make the raw data into an interpretable output that can be understood as a knee angle as well as an indicator whether CM is present. Then, this processed data is transferred and displayed on a visual interface.

## Justification for simplification of knee model

As described earlier, rotation around the transverse axis is the major function of the knee. However, two additional, passive movements contribute to the complexity of accurately modelling the knee joint.

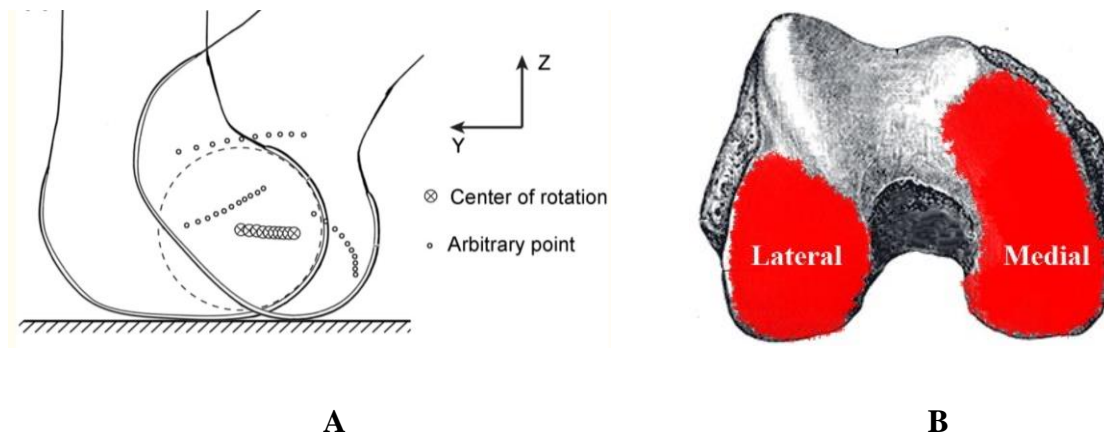


Figure 8 Rotation of convex femur on flat surface and resulting point of rotation (A), from (31). Inequality in femoral condyle sizes (B), from (32).

According to the Kaltenborn rule, as the tibia's condyles are concave and the femoral condyles are convex, flexion and extension also give rise to translation (Figure 8 A) (33). The following two cases describe translation movement on the sagittal axis driven by this anatomical property. If the convex femur is fixed e.g. in sitting on a chair, while the concave tibia rotates, flexion is accompanied by posterior translation of the tibia (open-chain). If the tibia is fixed e.g. in standing, while the femur rotates, flexion is accompanied by anterior translation of the femur (closed-chain).

As the lateral condyle on the femur is a smaller structure, its end is reached earlier during extension (Figure 8 B). Therefore, the only way to fully extend the leg, is for either the femur to perform a medial rotation (closed-chain) or for the tibia to perform an external rotation of  $10^\circ$  (32). This movement is called screw-home mechanism. This secondary movement can be observed when the last 30 degrees of extension are about to be performed and is caused by the anatomical differences of the condyles.

As described above, the knee does not rotate about a fixed axis. However, it might be that the translation in the sagittal axis has a negligible effect on the knee angle such that a simplification can be considered.

A simplified model of the leg is proposed. It has two beams and a revolute joint (R-model) as resemblance of the knee joint and is compared against one with an additional prismatic joint to account for the translation on the sagittal axis (RP-model). The baseline for the comparison is defined by the minimum requirement for spatial resolution, namely a change of  $10^\circ$ .

$$x = l_{shank} \cdot (1 - \cos(\alpha)) \quad \text{Equation 1}$$

$$y = l_{shank} \cdot \sin(\alpha) \quad \text{Equation 2}$$

$$d_{euc} = \sqrt{(\Delta x^2 + \Delta y^2)} \quad \text{From (34) Equation 3}$$

This angle can also be interpreted in the cartesian coordinate system as a change of x and y (Equation 1, Equation 2, Equation 3). By using a shank length ( $l_{shank}$ ) of 36 cm, any set of x and y resembling a change of knee angle ( $\alpha$ ) of  $10^\circ$  results in a Euclidean distance of 6.28 cm between end-effectors of the revolute-only model.

With this measure as the baseline, we can compare the two models and their RMSE values for a whole ROM trajectory. Therefore, the two models were designed using the Denavit-Hartenberg approach and the Matlab Robotics Toolbox by Peter Corke (35). Parameters for shank (36 cm), ROM ( $-10^\circ$  to  $110^\circ$ ) for both rotation and translation as well as an offset for translation (4 mm) were defined using anatomical literature (36)(37). Using forward kinematics, the x and y components of the end-effector for both models were tracked and then compared both graphically (Figure 9) and via the root mean square.

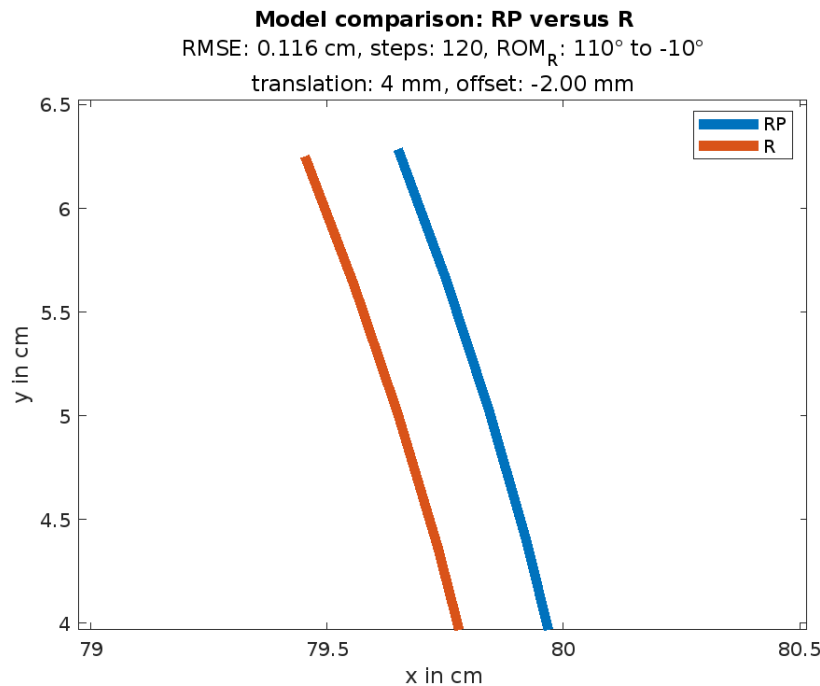


Figure 9 Comparison of revolute-prismatic and revolute model showing the deviation of end-effector position in the end-range of motion.

The RMSE between the models is 1.2 mm. Comparing the detected RMSE to the Euclidean distance of the needed resolution, the change in the model accounts for 2% ( $1.2 \text{ mm} / 62.8 \text{ mm}$ ) of the detectable angle. Therefore, in the next chapter, it is considered appropriate to replace a correct biomechanical model with a simplified structure.

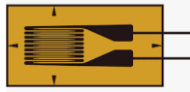


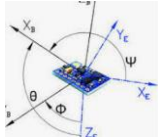






## Methods

The section describes all methods used to achieve the two objectives. Thereby, a design process is initiated for the first objective entailing three different concepts derived from the morphological map. Each of the concepts entails subparts namely concept description, verification methods and their results as well as a brief discussion. A concept decision paragraph concludes to continue with one of these concepts. Afterwards, the final hardware design is introduced, finalizing the first objective. Then, focusing on the second objective, the pathway from recorded signal to a classification is described.

# Concepts

It was decided to use three concepts in further detail that evolved out of brainstorming using the morphological map below (Table 3). These were all based on different sensors, namely a flex-sensor, a camera-sensor and an inertial measuring units (IMUs).

Table 3 Morphological map for brainstorming concept ideas. It is to be noted that each column does not indicate an optional design. Instead, in each row, one item can be picked to create a design.

Sensor	Strain gauge sensor 	fiber optic sensor 	Camera 	IMU 	Gear teeth 	EMG 	Kinect 
Design	Sock 	Two adhesive patches 	Two straps/brackets 				
Processing unit	Arduino	Rasberry Pi	Computer				
Visual Interface	Computer Monitor	Cell Phone	LED indicator				
Data transmission	Bluetooth	Wifi	Radio				
Programming language	C++	Matlab	Python	OpenSim			

In the following chapters, these ideas are presented and tested against the requirements.

## Idea 1a – Resistive flex sensor

This idea consists of two different kinds of flex-sensors namely resistive and capacitive flex-sensors.

### Concept

This preconcept is a fabric that is in the shape of a sleeve-sock, that is surrounding the knee entirely and tightly. A compartment on the anterior or lateral side of the fabric entails a flex-sensor (Figure 10 - A/B). When the sensor is bent, the resistance changes. In a voltage divider circuit, this change can be recorded and an analog to digital converter (Arduino Uno) can be used to map the change in resistance to the underlying angular displacement.

### Working principle

The sensor used for this subproject is SF15-150 from Fafeicy.

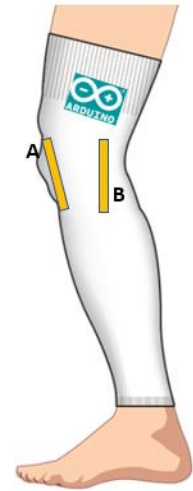


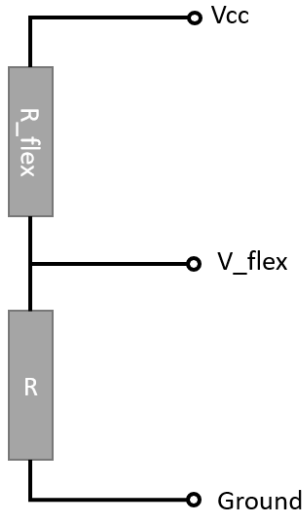
Figure 10 Preconcept with flex-sensor position either lateral or anterior



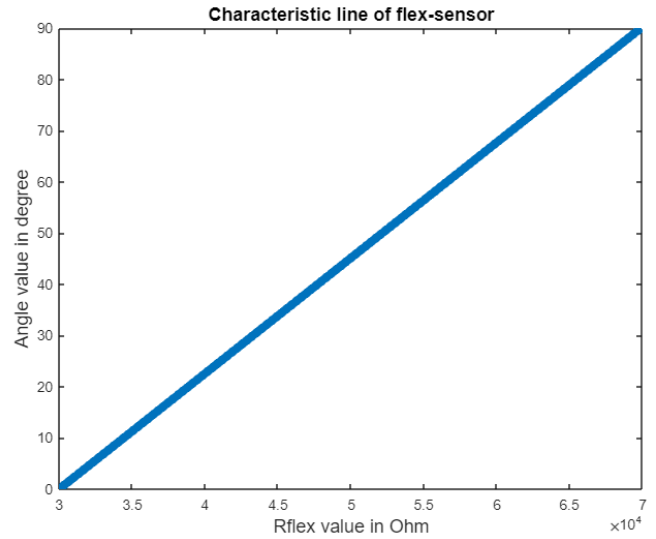
Figure 11 Close-up of resistive flex sensor (1) with flexible plates (A and B), and conductive elastomer (C). Bent flex sensor with conductive dots (red arrow) and plates (2)

The working principle relies on two metallic contacts which connect on either side to flexible plates (Figure 11 - 1 – A/B) along the length of the sensor. A conductive elastomer (Figure 11 - 1 - C) is situated between the two plates and is constituted of many small conductive dots (Figure 11 - 2). If the sensor is bent, the distance between the dots increases by which the resistance increases proportionally to the bending.

## Voltage divider



**A**



**B**

Figure 12 Voltage divider consisting of a known resistance  $R$ , known supply voltage  $V_{cc}$ , measured resistor voltage  $V_{flex}$ , and the unknown resistance  $R_{flex}$  (A), Theoretical characteristic line relating  $R_{flex}$  value and corresponding angular displacement (B)

$$\frac{V_{flex}}{V_{cc}} = \frac{R}{R+R_{flex}} \Rightarrow R_{flex} = R \cdot \left( \frac{V_{cc}}{V_{flex}} - 1 \right) \text{ From (38)}$$

Equation 4

With the known parameters  $V_{cc}$  and  $R$ , and the measured  $V_{flex}$ , Equation 4 yields  $R_{flex}$ .

Since the manufacturer determined a linear proportionality, two points of the sensor must be determined to draw the characteristic line via Equation 5.

$$\circ(R_{flex}) = m \cdot R_{flex} + b$$

From (34)

Equation 5

$$\text{with } P_1 = (0^\circ | R_{flex_{flat}}) \text{ and } P_2 = (90^\circ | R_{flex_{bent}}),$$

$$m = \frac{90^\circ - 0^\circ}{R_{flex_{bent}} - R_{flex_{flat}}},$$

$$b = 90^\circ - m \cdot R_{flex}$$

The two values were measured using a multimeter and the corresponding characteristic line yields the following results (Figure 12 - B).

## Setup and code

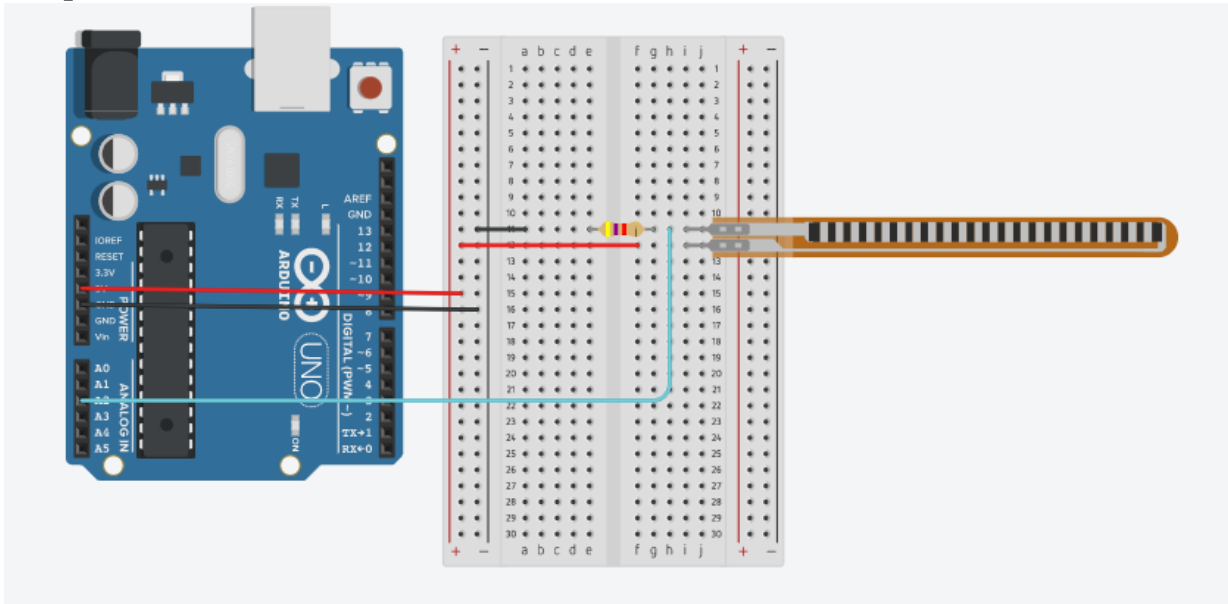


Figure 13 Voltage divider circuit with flex-sensor, breadboard and Arduino

This circuit in Figure 13 was simulated via TINKERCAD and later created. A C-code was written that indicates which analog pin receives data from the circuit and executes the conversion from  $R_{flex}$  to an angle.

### Initial testing

The sensor was hot-soldered (350 °C) to a set of jump-cables to allow for easier implementation of the sensor within the breadboard circuit. During initial testing, a problem arose that requires attention in future application of these sensors. Bending the sensor caused one contact to break. Possibly, the contacts became fragile through the soldering process. Also, the strain that acted on the contacts might have caused the same. To counteract this, possible measures could be to use a cold-soldering technique, clamp the contacts or to support the contacts (with e.g. rubber etc.) such that they do not directly take strain.

As opposed to continuation with the abovementioned sensor with a different construction, it was decided to take an off-the-shelf sensor that already considers the above with an elastomer casing.



## Idea 1b - Bendlabs capacitive flex-sensor

### Working principle

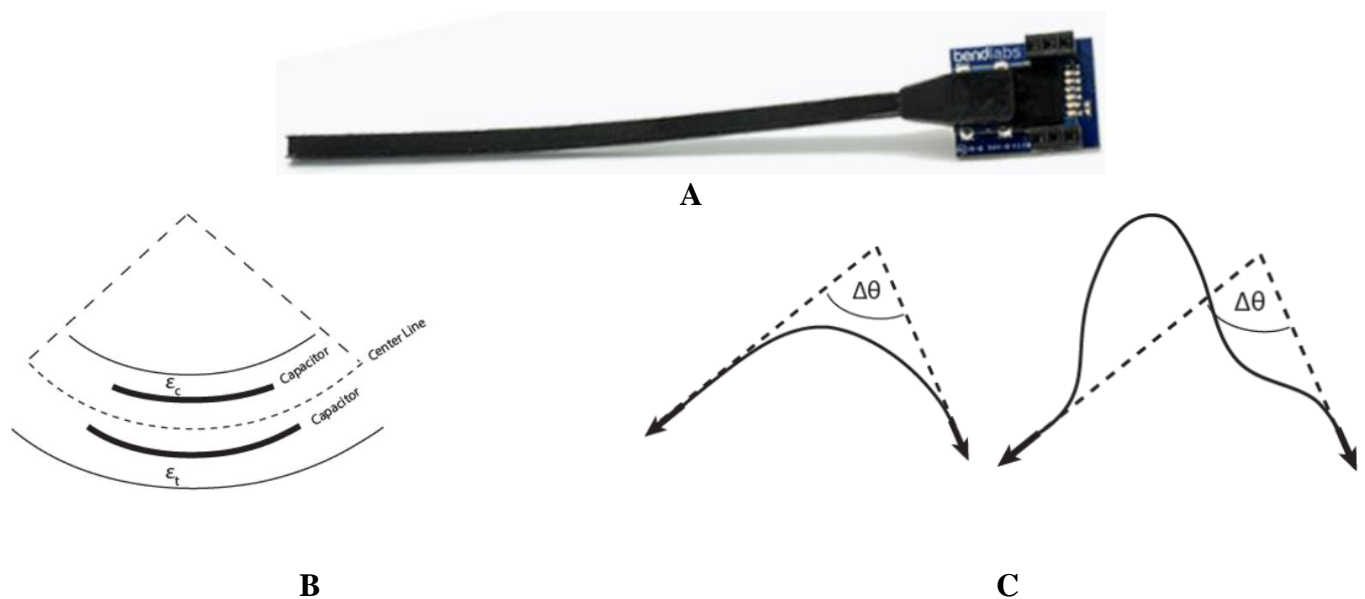


Figure 14 Bendlabs 2-axis flex sensor (A), Cross section view of the two-capacitor sensor with compressive strain  $\epsilon_c$ , the other tensile strain  $\epsilon_t$  (B). Schematic describing path independence, that means that both paths yield the same output (C). A, B, C from (39)

The bendlabs flex sensor (Figure 14 - A) utilizes a differential capacitance measurement. Comparing the flexion to a center line (Figure 14 - B), one capacitor experiences compressive strain  $\epsilon_c$ , the other tensile strain  $\epsilon_t$ . Since the sensor measures a differential capacitance, the sensor's technology decreases the impact of common tensile strain, the bending radius or the path that it takes (Figure 14 - C) on angle measurement. The latter property is due to the fact that the capacitors are situated along the entire length of the sensor. When calculating capacital difference, extra bends cancel each other out. Therefore, angular displacement is a variable only relying on the two vectors defined at the ends of the sensor. Another advantage of this sensor is the contact area which allows for a lateral measuring position - as opposed to the resistive sensor that could not be used in another direction.

### Verification

A simple mechanical structure with a revolute joint and two shanks was built to verify the angular measurement. As the sensor experienced tensile and compressive stress which in turn causes unwanted angular displacement throughout a period of repetitive movements, braces were 3D-printed that encapsulate the ends of the sensor. Additionally, this aligns the sensor with the structure. The structure was centrally placed inside an angle-indicating semi-circle and attached on a wooden board.

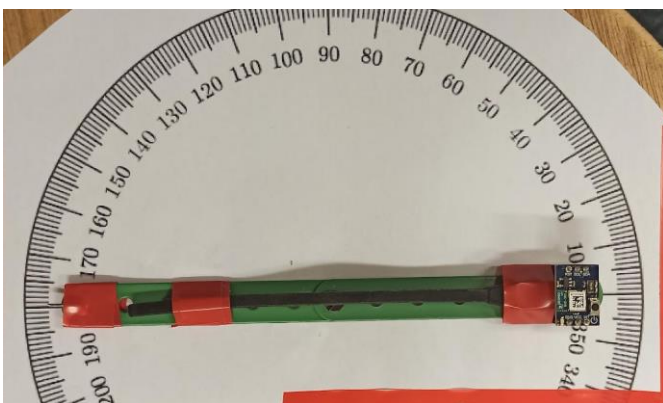


Figure 15 Flex sensor test setup with green mechanical structure consisting of two shanks and a revolute joint on a semi-circle indicating angles

A camera was positioned above the structure alligning the centerpoint with the rotation axis. In 10° steps, pictures where taken and lines were drawn to measure the angle (Figure 15). An online tool was used for measuring angles from pictures (40). All tested angles measured by the tool where coinciding with the semi-circle angles with 1° accuracy.

All following tests were performed using the Bend Labs Connect app on a Xiaomi Red Mi Note Pro 8 Plus.

**Exhaustive stationary test**

To see how much a long-held static angular position is deviating, two tests at -10° over 2 minutes with a sampling frequency of 100 Hz were conducted. Later, RMSE values were calculated with the static true value of -10°. Since the accuracy of the setup was 1°, the result was rounded to full degrees. Results were 1° RMSE for both datasets.

**Repetition plateau test**

To test the output consistency for repetitive motions (as posed by the squat task), pins were introduced into the wooden board that limit the ROM of the structure and make sure that the same position is taken each repetition. One limit was always defined by the current interval (true value), the other was set arbitrarily. Close attention was paid to gently execute each movement such that the pins do not deform.

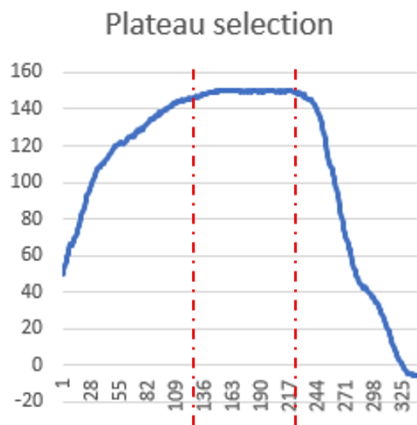


Figure 16 Recorded data for repetition plateau test tracked in blue over samples taken and the plateau period marked in red (left)

After recording, each hill was separated (Figure 16), the plateau periods were fused and RMSE-values were calculated on the basis of the true value. The accuracy was tested in 10° intervals (Table 4).

Table 4 RMSE-results for repetition plateau test for full ROM in 10° intervals

true value in °	RMSE in °	true value in °	RMSE in °
-10	1	80	4
0	1	90	0
10	3	100	1
20	6	110	2
30	6	120	2
40	2	130	2
50	3	140	2
60	2	150	3
70	1		

*Discussion*

The first test shows that even in the entirely stationary case, the output can have an RMSE of 1° (Table 4). This deviation could stem from drift, the oscillation of the output or digitisation within the process.

The second test shows that the error following a repetitive movement is not the same throughout the whole range. The greatest RMSE was seen at 30° (6°), the smallest at 90 degrees (0°). That means that if the output angles are later used for decision-making, we need to consider the value of it and maybe readjust thresholds to account for the different uncertainties.

## Idea 2 - Inertial measuring unit

In the following section, the inertial measuring unit (IMU) concept is described in detail, after that a description about the working principle and verification is done.

### Concept

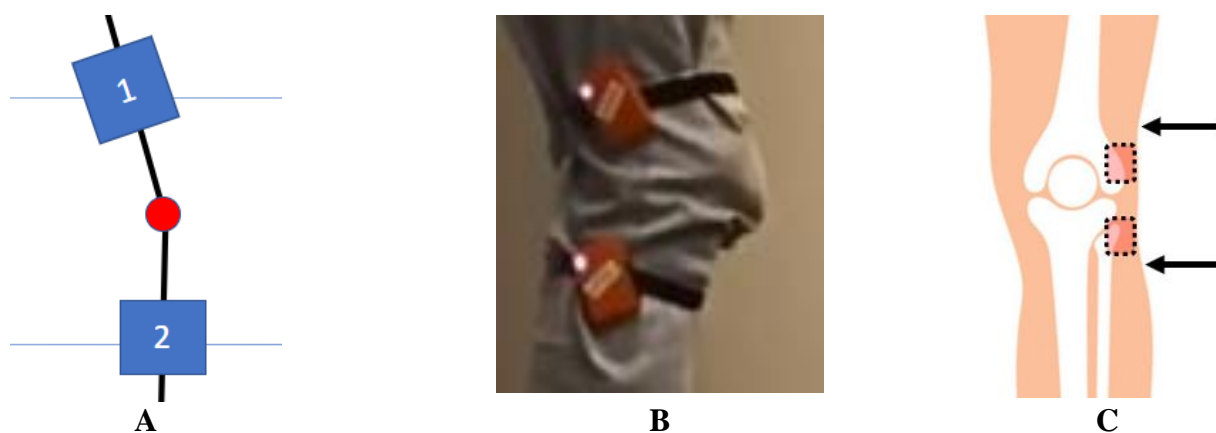


Figure 17 Schematic indicating how angles can be measured from the two IMUs (A), initial setup with straps (B), Knee schematic indicating in red the anatomical landmarks (distal end of femur for thigh-IMU and head of fibula for shank-IMU) by which the IMU positions shall be determined (C)

For this concept, one inertial measuring unit is positioned on the upper and lower leg respectively (Figure 17 - A/B). They should be positioned with straps. Since they individually record data about their rotation referring to the global reference frame, their difference on the Y-axis (pitch) defines the knee angle.

Both IMUs shall be positioned by their relation to anatomical landmarks. The lower-leg IMU (shank-IMU) shall be positioned 1 cm below the head of the fibula, which can be located by palpating the lateral side (Figure 17 - C). The upper-leg IMU (thigh-IMU) shall be positioned 1 cm above the distal end of the femur. These positions were chosen to be on the lateral side and close to the knee for several reasons.

### Lateral side

They should be rotatable about the Y-axis to account for calibration angle (does not work for anterior and posterior side). None of the medial surfaces is big enough to provide space for the IMU. Here it is to say, that the medial plane poses a specific problem since the gastrocnemius (calf muscle) and tibia intersect abruptly which might make the sensor slide from the medial to the anterior-medial plane defined by the tibia. In this case, the calibration pitch angle cannot be guaranteed. Additionally, all other sides (including medial) express more muscle tissue. After movement execution, they vacillate causing inaccuracy.

### Close to the knee

According to the formular of centrifugal force (Equation 6) which entails centrifugal force  $F$ , mass  $m$ , angular velocity  $\omega$  and distance  $r$ ,

$$F = m\omega^2r, \quad \text{From (38) \quad Equation 6}$$

the further the IMUs are positioned from the point of rotation (knee), the more force will be exerted onto them. In a seated kicking task, the shank-IMU will be more effected by it, in a squat-task, the thigh-IMU will be. It might be that the force causes transient (immediately after movement) or permanent dislocation of

the sensors. For that reason, the IMUs shall be placed as close as possible to the knee on both lower and upper leg. This is also in line with (41).

### Working principle

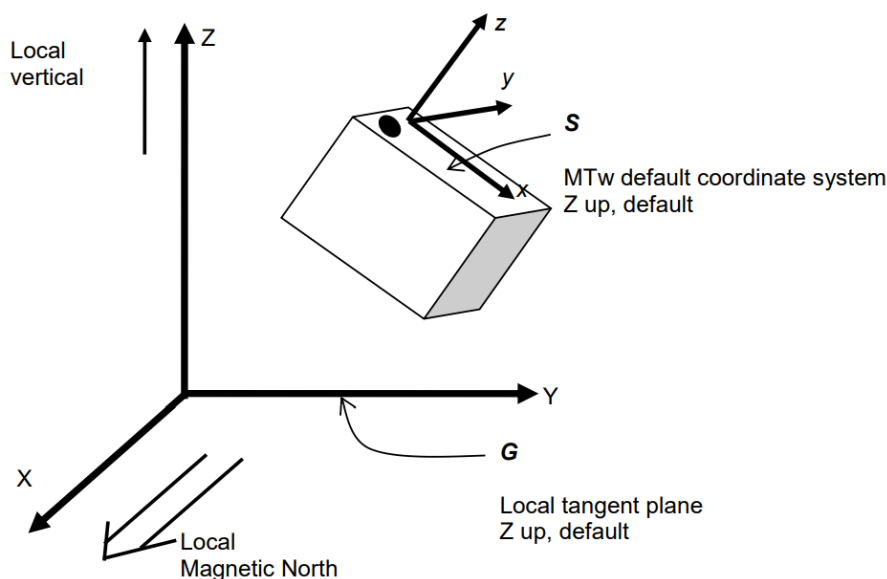


Figure 18 Coordinate system showing the global North-west-up global frame and the local IMU-frame relative to it. From (42)

The inertial measuring unit (IMU) system used for this project is the MTw Awinda MW111415/3.0.6 from Xsens (Figure 18). The system entails a station (Awinda station) that communicates with individual sensor units (each an IMU) via radio frequency of 2500 MHz. Each IMU has an accelerometer measuring 3D inertial data, a magnetometer measuring 3D magnetic field strength, and a gyroscope measuring orientation. A sensor-fusion algorithm called “Xsens Kalman Filter for 3 degrees-of-freedom orientation for Human Motion” uses these inputs to compute accurate 3D orientation and can output these as different descriptors (e.g. roll, pitch, yaw). (42)

While the accelerometer detects gravity and can thereby define the orientation on a plane orthogonal to it (roll and pitch), the magnetometer provides information about true north and can thereby determine the offset (yaw). This procedure to fully determine orientation of the IMU is only suitable for the stationary case. In any other case, the accelerometer will pick up non-gravity information and still interpret it as such. Therefore, the gyroscope is additionally used to provide a full description of orientation. It is to be emphasized that due to this working principle, the outputs of the IMUs are always referring to an earth-related north-west-up frame. (42)

### Gimble lock problem

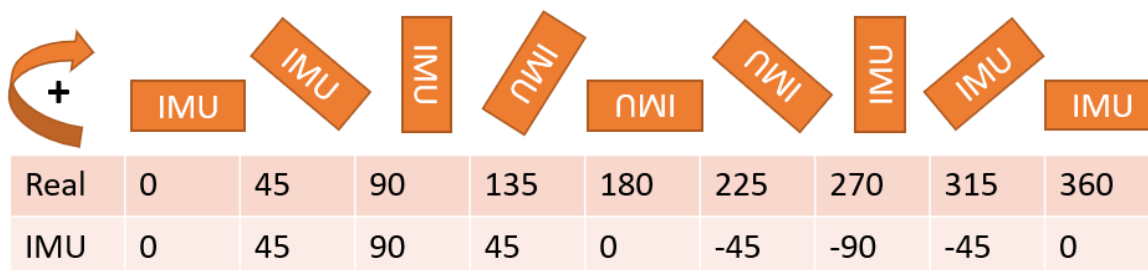


Figure 19 Rotation of IMU around y-axis with real rotation and IMU value

When tracking each individual output namely roll, pitch, and yaw angles, it was seen that the pitch angle has a range of  $-90^\circ$  to  $90^\circ$ , whereas roll and yaw range from  $-180^\circ$  and  $180^\circ$ . That means that all values which

are part of the ranges  $-90^\circ$  to  $0^\circ$  and  $0^\circ$  to  $90^\circ$  are displayed twice within the full rotation around the y-axis (pitch) (Figure 19). Therefore, the representation of the angle is not unique. This is due to a singularity phenomenon called gimble lock.

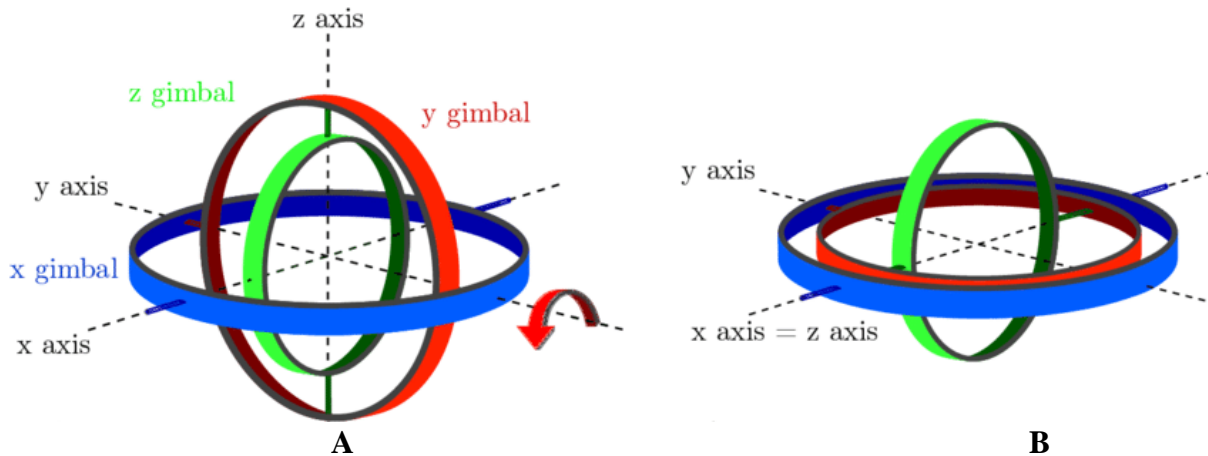


Figure 20 Coordinate system designed to replicate wholesome rotations in 3D space (A). Gimble lock condition by two coinciding axes (B). From (43)

There are many ways to define rotations in three-dimensional space. One of them is via Euler-angles which is the most intuitive representation. In essence, the Euler-angles define a sequence of rotations (e.g. X, Y, Z) about each of the orthogonal axes. This sequence is hierarchical namely every change of the first axis changes the other two accordingly. Due to this definition, if the mid-sequence axis coincides with the outer-axis, one degree of freedom is lost. That means that angular displacement of either of the axes expresses the same rotation. When abstracting the rotation sequences into rotation-matrices, the occurrence of DOF-loss can be described in another way.

Defining a 3D coordinate system with the axes x, y and z, a rotation  $R$  could be described by three consecutive rotation matrices ( $R_x, R_y, R_z$ ) with a designated rotation each, namely  $r = \text{roll}, p = \text{pitch}$  and  $y = \text{yaw}$ .

$$R = R_x(\text{roll})R_y(\text{pitch})R_z(\text{yaw}) \tag{Equation 7}$$

Since every rotation matrix is defined as a singular rotation around one axis only, with  $c(x) = \cos(x)$  and  $s(x) = \sin(x)$ , we yield

$$R = \begin{pmatrix} 1 & 0 & 0 \\ 0 & c(r) & -s(r) \\ 0 & s(r) & c(r) \end{pmatrix} \begin{pmatrix} c(p) & 0 & s(p) \\ 0 & 1 & 0 \\ -s(p) & 0 & c(p) \end{pmatrix} \begin{pmatrix} c(y) & -s(y) & 0 \\ s(y) & c(y) & 0 \\ 0 & 0 & 1 \end{pmatrix}. \tag{Equation 8}$$

If the mid-axis is now turned by  $p = \frac{\pi}{2}$ , we yield

$$R = \begin{pmatrix} 1 & 0 & 0 \\ 0 & c(r) & -s(r) \\ 0 & s(r) & c(r) \end{pmatrix} \begin{pmatrix} 0 & 0 & 1 \\ 0 & 1 & 0 \\ -1 & 0 & 0 \end{pmatrix} \begin{pmatrix} c(y) & -s(y) & 0 \\ s(y) & c(y) & 0 \\ 0 & 0 & 1 \end{pmatrix}. \tag{Equation 9}$$

Executing matrix multiplication and using trigonometric identities

$$s(a \pm b) = s(a)c(b) \pm c(a)s(b) \quad \text{Equation 10}$$

$$c(a \pm b) = c(a)c(b) \pm s(a)c(b) \quad \text{Equation 11}$$

yields

$$R = \begin{pmatrix} 0 & 0 & 1 \\ s(r+y) & c(r+y) & 0 \\ -c(r+y) & s(r+y) & 0 \end{pmatrix}.$$

Equation 12

The outcome is the fusion of the angular displacement about the x-axis. (44)

This condition is by definition a problem of Euler-angles, not of the system itself. A few solutions can be proposed to solve this issue:

1. Another representation for rotations can be used such as quaternions. These do not give rise to this problem.
2. Calibration can be used to position the singularity in a state that is not reached by the task.

Since the output of the system shall be an angle, solution 1 would be just a conversion into another language. When transforming back into angles, the same problem would maintain. To avoid this, another project transferred the rotation matrix information into a biomechanical model. The readout of the biomechanical model was without singularity-problems. The problem with this approach however is, that they needed to always setup and calibrate all 17 IMUs (45). Therefore, solution 2 was chosen.

## Sitting calibration

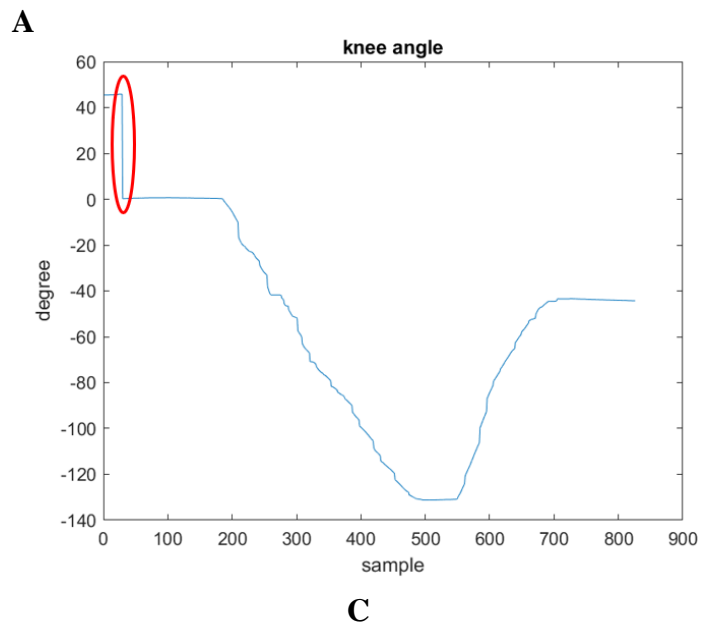
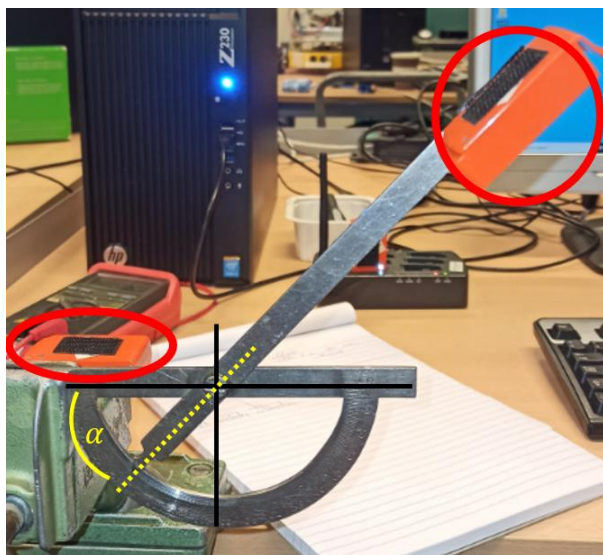
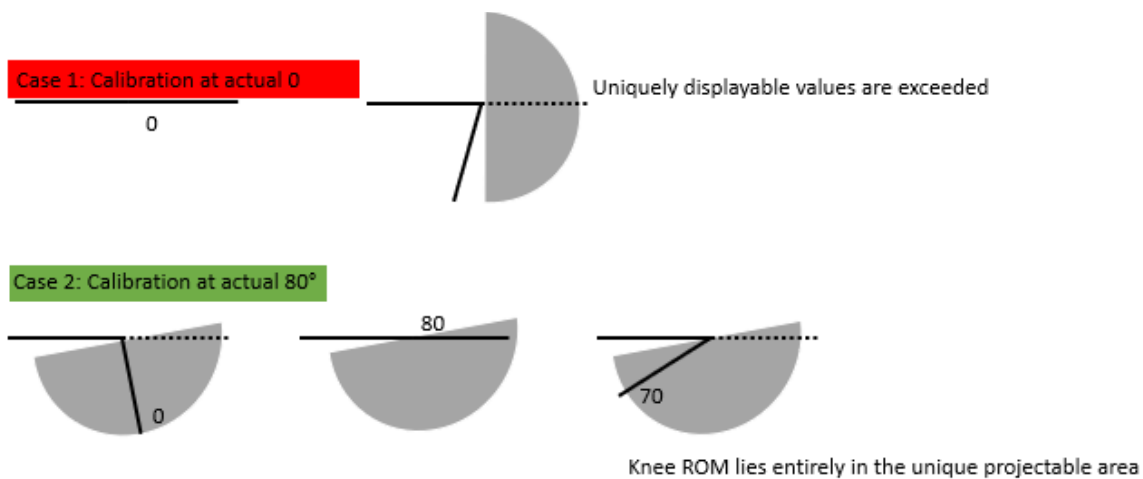


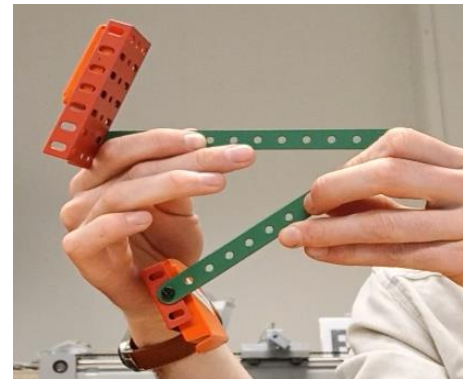
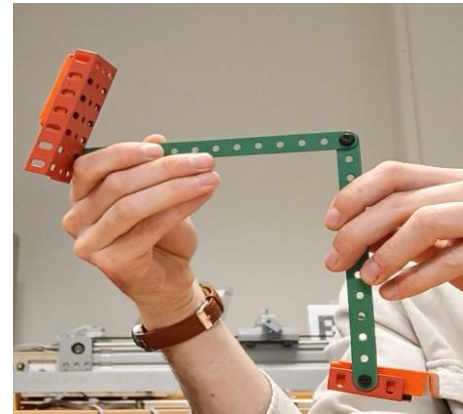
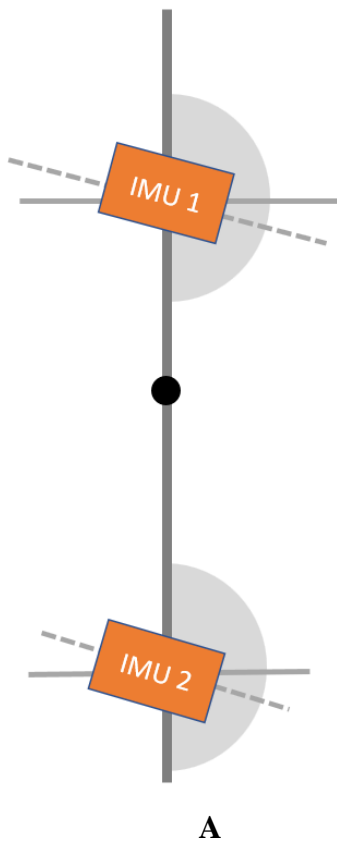
Figure 21 Graphical explanation for calibration as a solution for not reaching singularity for the seated kicking task and squats (A). Setup for calibration testing. While the two red circles indicate the IMUs, yellow indicates the calibration angle (B). Plot of knee angle over samples, where the red circle indicates the moment of calibration which was set to 30 values (C).

While the knee-ROM in case 1 exceeds the range of uniquely displayable values, calibration at a close-to-90° value in case 2 allows for the ROM to be entirely shown (Figure 21 - A).

A test-setup was created to verify that a post-calibration value of 0° is present (Figure 21 - B). Thereby, defining the position at calibration angle as the new 0°. To acquire, calculate and display calibrated knee-angle, a Matlab-function was developed based on the function “mainMTwRTdataViewer” available from Xsens’ website (46). The mean of the first 30 knee angle values was used as the calibration value that was deducted from all following output values (Figure 21 - C).

This calibration procedure demands the patient to perform a full-extension (0°) in a seated-position for a prolonged time to be sure that the only angle measured is the actual calibration offset-angle. However, patients are not expected to be able to reach this angle (0°) and if so, not for long. Therefore, another calibration procedure was tested.

## Standing calibration



Sensor and knee angle tracking

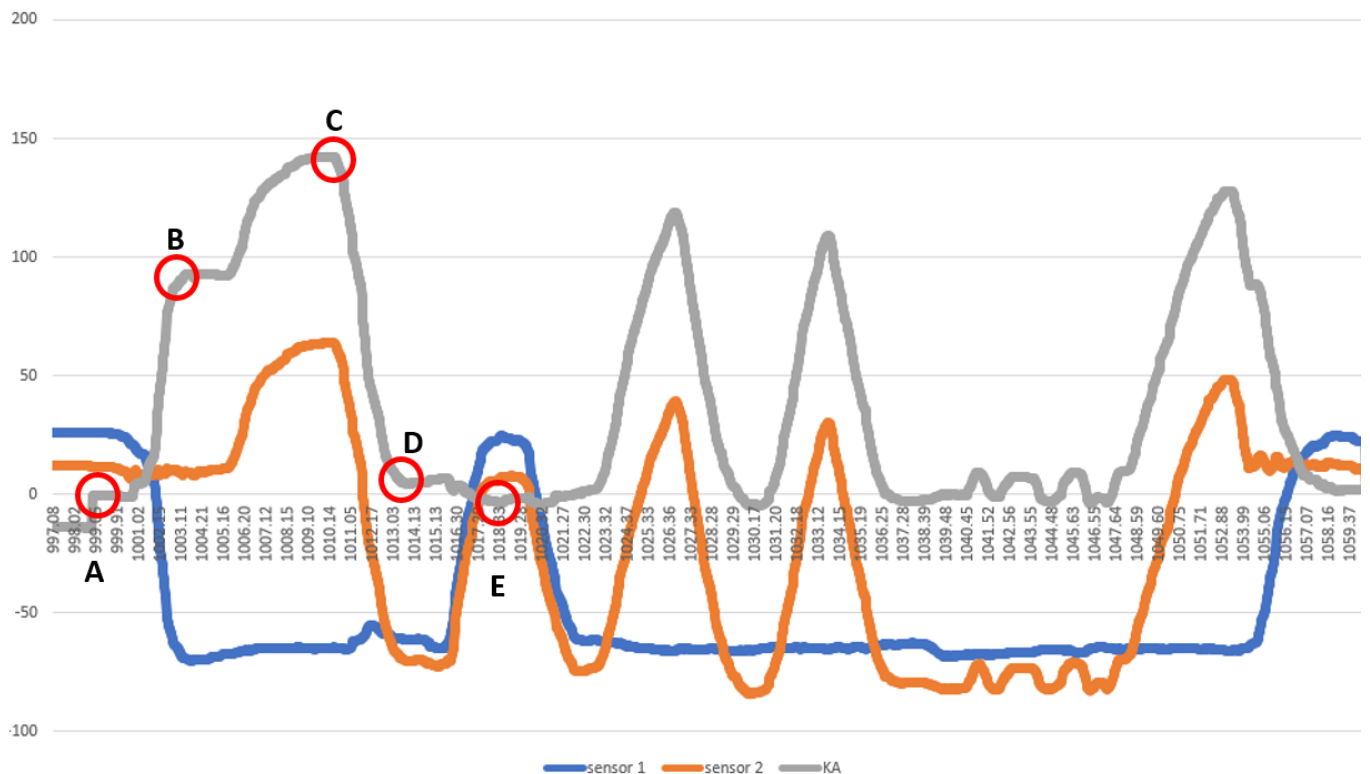


Figure 22 Schematic view of IMUs in standing position with uniquely displayable angular displacement interval in grey (A), calibration testing device in standing position (A.2), in seated position (B), in maximal flexion (C). Plot of sensor 1, sensor 2 and knee angle calculation data over time (bottom) with point of full extension in seated position (D) and locked-angle rotation from seated to standing position (E).

In the standing calibration, the patient is asked to fully extend his/her leg to receive a 0° measurement (Figure 22 A and A.2). Figure 22 - bottom shows that standing (A), 90° flexion (B) and full flexion (C) are



reflected in the measurement. Moreover, the transition from sitting 0° (D) to standing 0° (E) cancels out in the knee angle which was also desired.

### Verification

The tests performed are regarding sampling frequency, stationary position, accuracy for 1 Hz change and pitch swing.

### Sampling frequency

A setup was created to check the accuracy. It entailed a camera and a goniometer with an accuracy of 1° for ground-truth measurements. The IMUs were attached via Velcro. Both IMUs and camera (smartphone Xiaomi Redmi Note Pro 8) recorded with a sampling frequency of 50 Hz. In the first test, three cycles from 0 to 90° were tracked. After recording, every picture of the camera output was analyzed and whenever the indicator needle of the setup was on a full degree, the frame number and degree were noted.

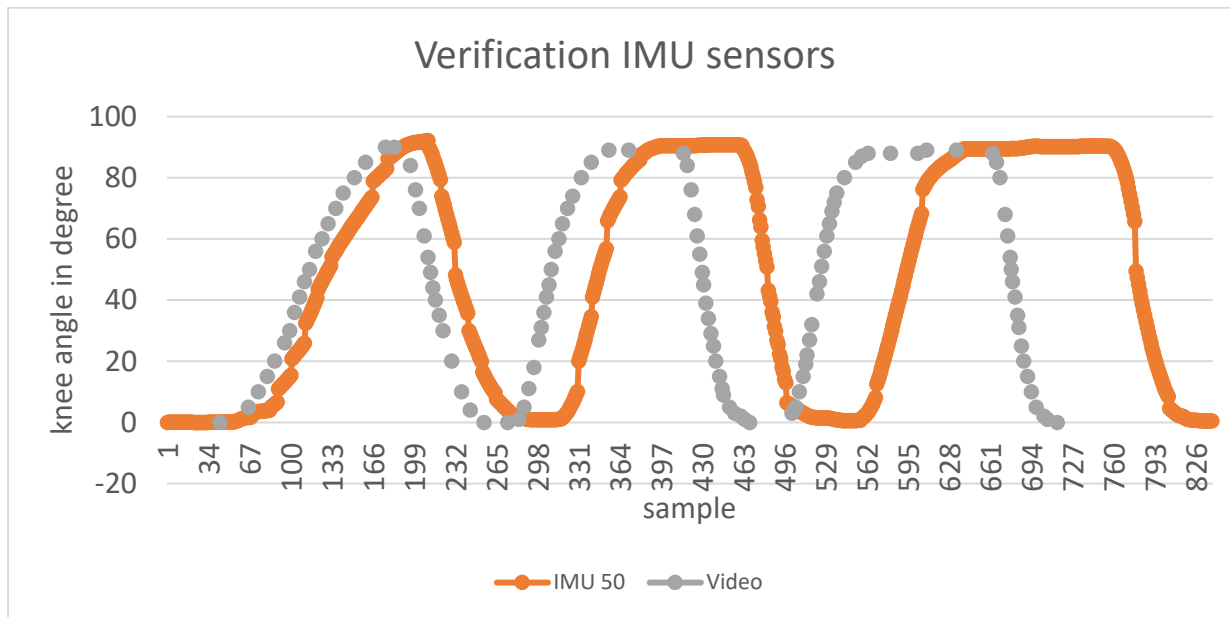


Figure 23 Video and IMU data for three movements from 0° to 90° plotted against samples

When tracking the results over samples (Figure 23), the data of video and IMU were not temporally coinciding. That might be due to package loss and communication issues on the IMUs. Although NAN-values were not present within this dataset and the Xsens claims to indicate data loss with such, jumps within the signal might suggest an inconsistent sampling frequency (e.g. in Figure 23, sample 780). Another possible source of error is the manual angle selection process for the camera which might have also caused inconsistencies.

Timestamps were used instead of sample-numbers trying to solve this issue.

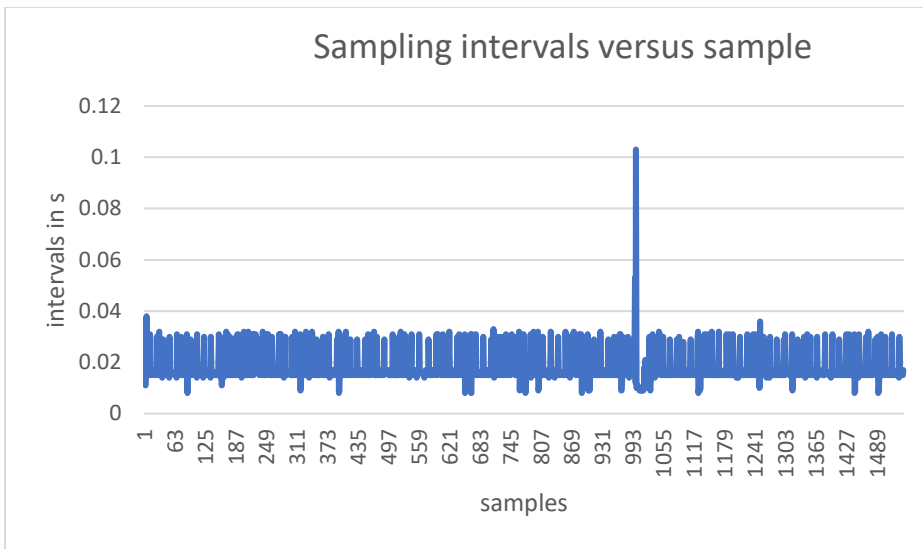


Figure 24 Between-sample intervals versus samples of IMU data

The timestamps entailed deviating inter-sample durations (Figure 24). When plotting the between-sample interval duration over samples, the highest durations are multiples of 1000 packages – this corresponds to the sample at which a structure in MATLAB is read to plot the graphs. For that reason, RMSE-comparison of live-data in this setup is not feasible since the camera used was not synchronized with the IMU acquisition. Therefore, it was decided to only rely on verification techniques which are not dependent on timestamp-data. All following tests were made with a sampling frequency of 60 Hz.

### Stationary test

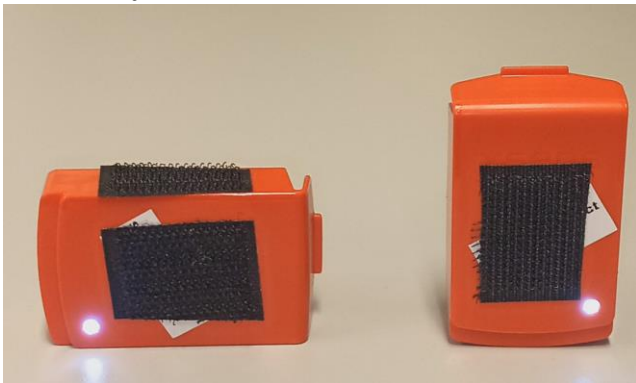


Figure 25 Position of IMUs for the stationary test

The sensors were kept in a steady position for more than 60 seconds (Figure 25). This duration was chosen since this equates the time necessary for one full cycle of task execution. The readings should be consistent throughout and in-between the recordings (Figure 26).

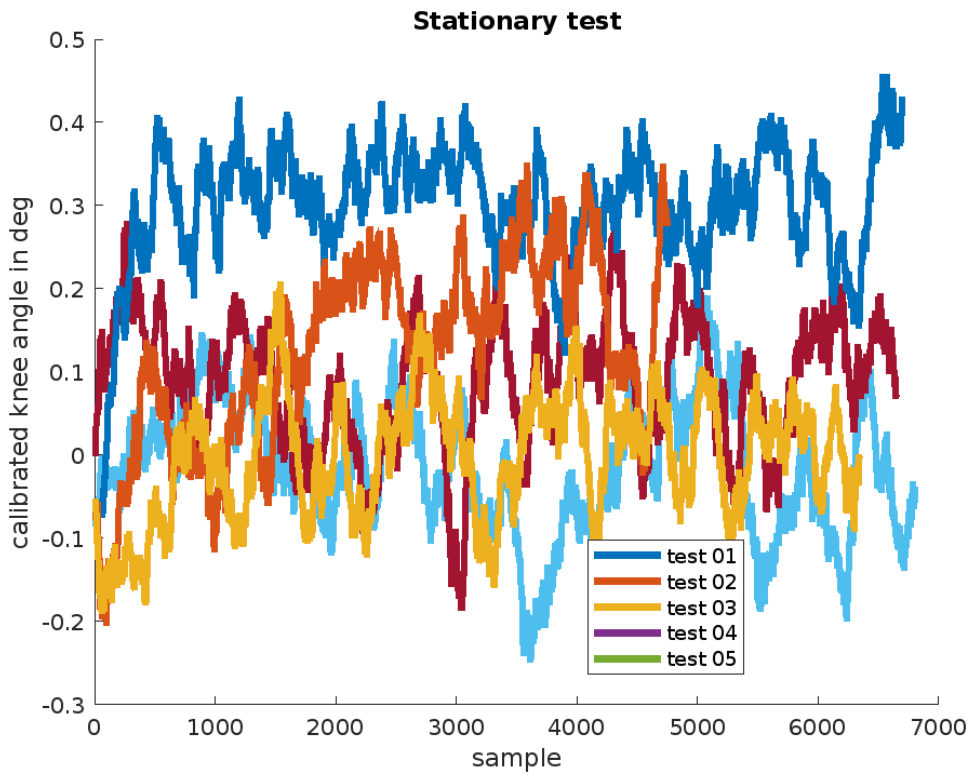


Figure 26 All five test runs for stationary test

To quantify the deviation from the actual value, RMSE can be used. In this case, the estimator is the true value of  $0^\circ$  since calibration was used (Table 5).

Table 5 Results for 5 tests to check the stability of the calibrated outcome in a stationary setting. Results are rounded to  $1^\circ$  accuracy.

test	#values	RMSE in $^\circ$
1	7000	0
2	6844	0
3	6897	0
4	4946	0
5	6539	0

### Pitch swing

While the sensors were attached via Velcro to a rigid structure with a between-IMU angle of approximately  $0^\circ$ , the entire structure was moved  $\pm 45^\circ$ . Regardless of the absolute difference to  $0^\circ$ , the measured knee angle should maintain the same value (Figure 27).

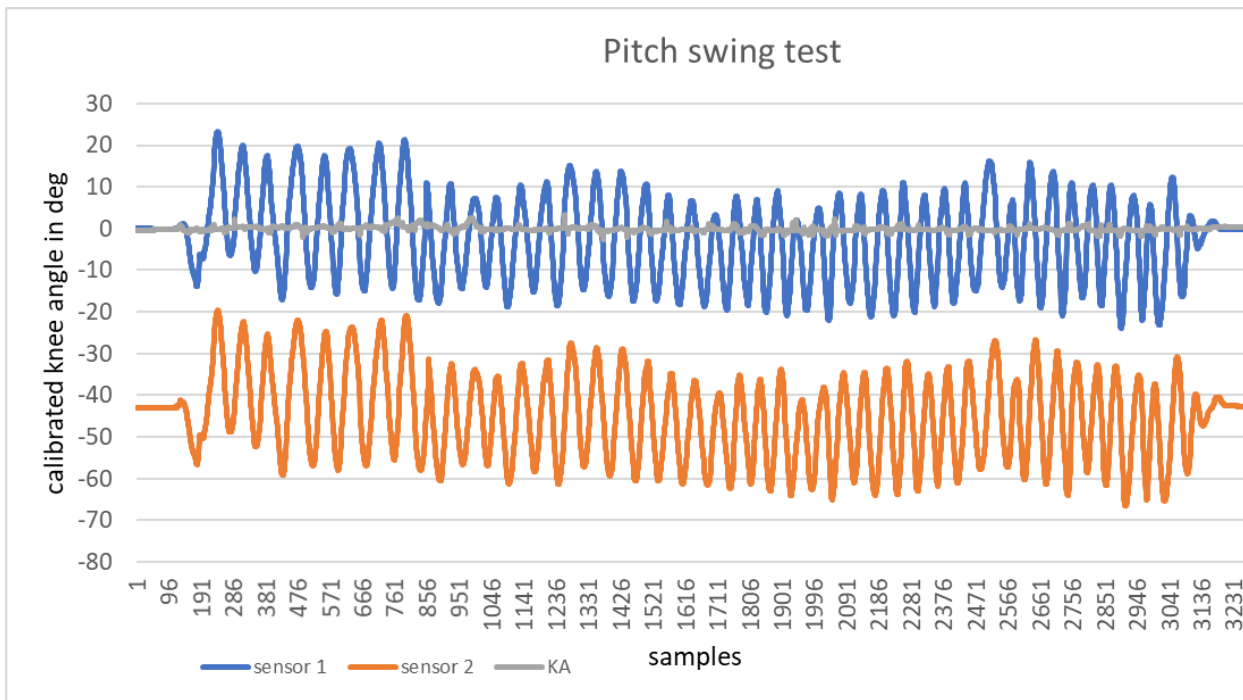


Figure 27 Pitch swing test plotted data indicating that if both IMUs are swung in the same way, when calculating the knee angle their individual movement cancels out (KA = knee angle)

Again, the root mean square error was used to quantify deviation. The estimator used was the mean of the initial post-calibration pre-movement period. The outcome was an RMSE of 1°.

### Metronome

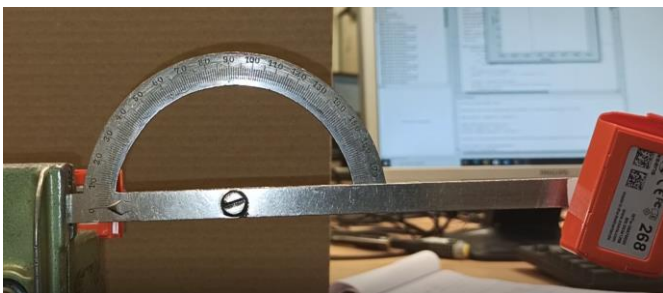


Figure 28 Setup for metronome test entailing two IMUS (orange) and a goniometer with 0° to 180° range

One IMU was placed level on the table, while the other was attached to a goniometer (1° resolution) in calibration-position (Figure 28). With 1 Hz, the attached IMU was moved within the full ROM. Simultaneously, a video was recorded for ground truth measurement. Every second, a static value was executed and noted. A simple Matlab-code was written for analysis, finding the values indicated by the video-reading and calculating the deviation from the IMU value (Figure 28).

Table 6 IMU metronome test results with 95 angles total

test	1	2	3	4	5	total
angles	21	20	16	22	16	95
RMSE in °	1	2	2	1	2	1

After five tests, treating all measurements as one, the total RMSE compared to the video ground truth is 1° (Table 6).

### Discussion

In order to assess whether the sensor system in combination with the calibration cascade qualifies for this project, three tests were conducted namely a stationary accuracy test, a swing test, and a full-ROM test. The highest RMSE from the stationary test was 0° (rounded) over 60 seconds of recording time. This implies

that there are almost no drift or noise are present. The pitch swing test had a RMSE of  $1^\circ$  which suggests that the system is capable of detecting knee angles regardless of the orientation of the whole leg. The metronome-test covered the whole range of motion ( $-10$  to  $150^\circ$ ) and had an overall RMSE of  $1^\circ$ . This implies that the system is capable of producing angle outputs within the requirement of this project ( $RMSE < 10^\circ$ ) even in task execution conditions. A limitation of this setup is the reading error due to parallax error.

### Idea 3 - Camera

#### Concept

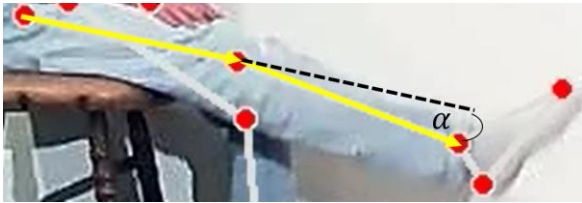


Figure 29 Hip-knee and knee-ankle vector span the knee-angle  $\alpha$

A camera (nor-tech Model 39278 with a resolution of  $640 \times 480$  px and a framerate of 30 fps) in combination with a convolutional neural network algorithm was tested to detect knee angle (Figure 29). A python code (v3.9.4) was developed that utilizes the MediaPipe Pose (v0.7) and OpenCV (v4.5.5) library for single-person pose estimation.

#### Working principle

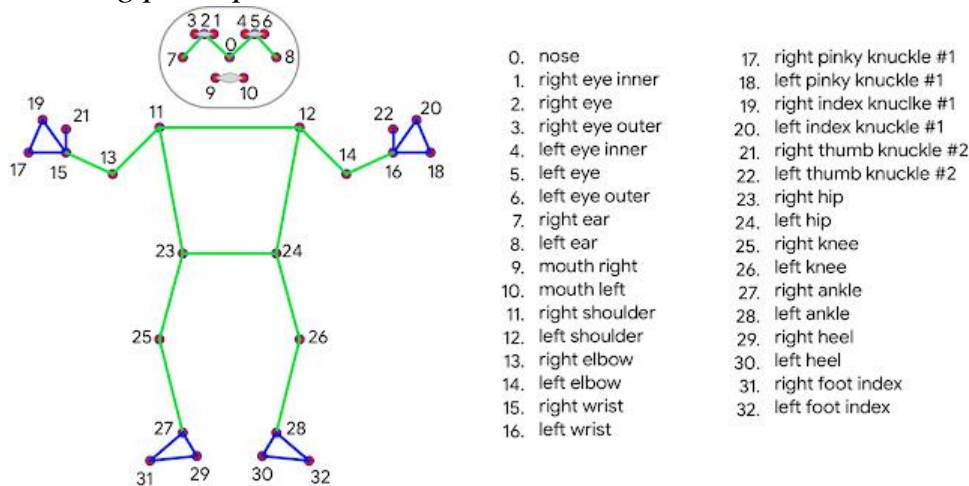


Figure 30 BlazePose body model as utilized by mediapipe. From (47)

The mediapipe pose library uses the BlazePose body-topography entailing 33 body location landmark (Figure 30). The first part of the algorithm revolves around finding a region of interest (ROI), i.e. the part of the picture that entails a person. The algorithm bases the presence of a human body on the assumption, that in all use-cases a face is visible. Since it is a body part with high-contrast features, it is a strong signal within the neural network and hence a good indicator to determine the ROI (47). The second part of the algorithm accounts for a problem in recent models which suffered from loss of accuracy in cases of occlusion or rare body positions (48). The used algorithm intelligently employs heatmaps and regression to find the best keypoint locations. This is done via a convolutional neural network estimating each keypoint's location with a certainty output (heatmap). Then, lower certain outputs are counteracted by using the other, more certain keypoints as predictors (regression). Differently put, low confidence of the heatmap output is compensated by a priori contextual information (human anatomy) (49). Each landmark has four outputs namely three positional (x, y, z) and one for visibility (occlusion yields a low score).

Joint metadata was extracted via the x and y output, and the knee-angle ( $\alpha$ ) was calculated by the two vectors hip-knee ( $v_{hk}$ ) and knee-ankle ( $v_{ka}$ ) using this Equation 13.

$$\alpha = \arccos\left(\frac{v_{hk} \cdot v_{ka}}{|v_{hk}| \cdot |v_{ka}|}\right) \quad \text{Equation 13}$$

Since this approach demands both the pose detection (detection of human) and tracking (tracking of hip, knee and ankle) to achieve a knee angle output, it was optimized to always show an output of the features described. This was achieved by setting the parameters MIN\_TRACKING\_CONFIDENCE and MIN\_DETECTION\_CONFIDENCE to 0.5.

### Verification

Three tasks were performed, namely

- Kicking: seated extension-flexion movement with a frequency of 0.5 Hz
- Seated: stationary position seated (close to 90°)
- Standing: stationary position standing (close to 0°)

to test on parameters such as the offset from a side-view, outfit and light-conditions.

### Setup, task and parameter descriptions

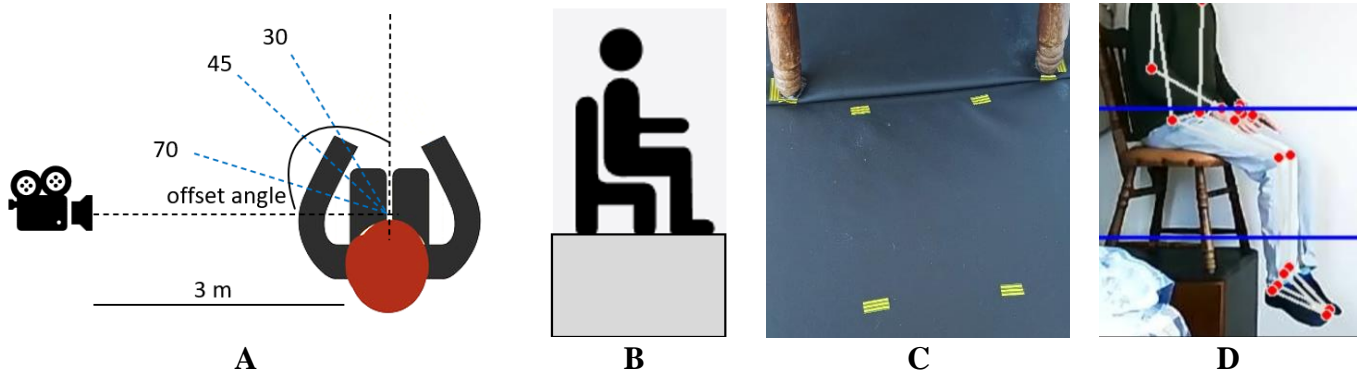


Figure 31 Setup for camera verification task in top-view (A): Blue dashed lines indicate offset angle. Side-view (B): Participant sits on chair on top of moveable box shelf (grey box). Markings indicating where to place feet and chair on moveable box shelf (C). Blue, directive lines used to ensure alignment (D).

The participant was placed 3 m away from the camera (Figure 31 - A). For the kicking and seated task, the following setup was used. The participant sat on the chair which was on top of the moveable box shelf (Figure 31 - B). He sat with a straight back, about to touch the backrest (Figure 31 – B/D). One of the edges of the box was aligned with markings on the ground for the offset-angle test (Figure 31 - A). Feet and chair were placed according to markings on the box (Figure 31 - C). For the standing task, the markings of the previous tasks were used to indicate foot position. The camera’s position was levelled by placing lines on the output live feed and aligning these with the surroundings (Figure 31 - D).

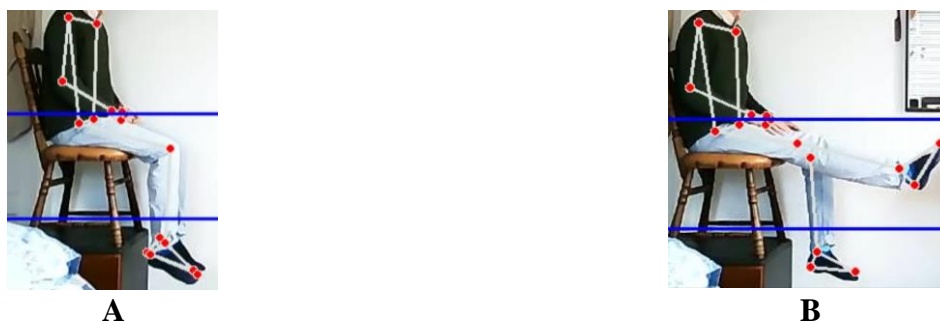


Figure 32 Participant with detected landmarks seated on chair with flexion (A) and extension (B)

In the kicking exercise, every second a metronome indicated change from up to down position or vice versa. Up-position was defined by fully extending the leg (Figure 32 - B), trying to maintain stationary until the metronome indicated the start of the consecutive movement. Down-position was defined by heel-touch with the box (Figure 32 - A). Defining full-extension as 0° and flexion as 90°, the peak-value should be close to 90°, whereas the valley value should be close to 0°. The kicking movement was performed 15 times. In the seated task, the feet were positioned roughly at 90° according to a mark on the box (Figure 31 - C). The seated subject was placed on a moveable box shelf such that it was easier to maintain the same rotations when changing the offset angle. Markings on the floor indicated how far the furniture needed to be rotated. In the standing task, the knee was locked in full-extension (0°).

Since the mathematical formula that is the basis of the knee angle calculation assumes a side-view, it was checked how the error increases when this assumption is violated. The kicking task was executed 15 times per offset angle (OA), standing and seated task were executed for one minute. In the kicking task, the maximum OA was tried to find beyond which no meaningful knee angles (RMSE<10°) were collected. A python code was written to extract peaks (flexion) and valleys (extension) of the signal per OA. Then, RMSE was calculated with estimators 90° and 0° for flexion and extension respectively. Another test was to wear different outfits to check if the algorithm works similarly good on all. Since the algorithm entirely relies on RGB-pictures, it is hypothesized that it works better in good lighting. Therefore, day, well-lit night and low-lit night conditions are compared for a one-minute recording each.

## Parameter 1 – Offset-angle Kicking

Table 7 Root mean square error (RMSE) and number of detected valleys (0°), peaks (90°) per OA for kicking task.

offset angle	RMSE peaks	num of peaks	RMSE valleys	num of valleys
90	6	15	2	14
80	8	15	2	14
70	13	16	10	14
60	13	15	11	14
45	26	16	11	15
30	38	16	13	14
10	27	1	5	12
0	66	15	2	14

The results in Equation 7 show that flexion error (RMSE peaks) increases for higher OAs, while extension error (RMSE valleys) increases until 30° OA and drops afterwards again.

The other tasks were performed from 70° to 90° offset angle since the ideal position is unlikely to be violated this much since human perception can distinguish non-right angular arrangements well enough (50).

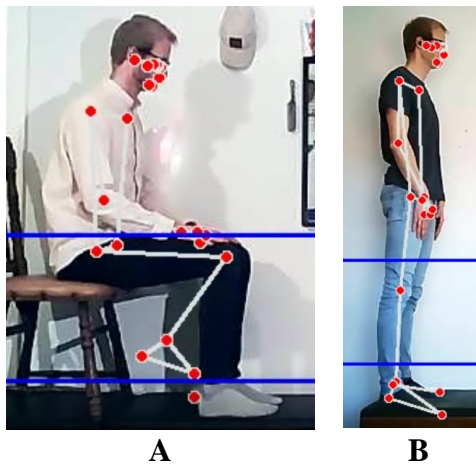
## Seated and standing

Table 8 RMSE results for seated and standing OA test.

OA in °	sitting RMSE in °	standing RMSE in °
90	1	1
80	2	1
70	5	1

In the seated position, increasing offset angle increases the error (1 ° to 5°) (Table 8). In the standing position, increasing offset angle did not have a consistent effect on the error.

**Parameter 2 – outfit**



	bright socks	dark socks	bright pants	dark pants
<b>Avg in °</b>	1	3	88	92
<b>Std in °</b>	0	0	2	7

Figure 33 False detections for ankle in black-pants (A) and toes in black socks (B), results for average and standard deviation for dark-bright pants and socks (C)

Judging from the higher standard deviation over the plateau period while seated (Figure 33 - A), wearing dark pants decreased the accuracy (bright 2° and black 7°).

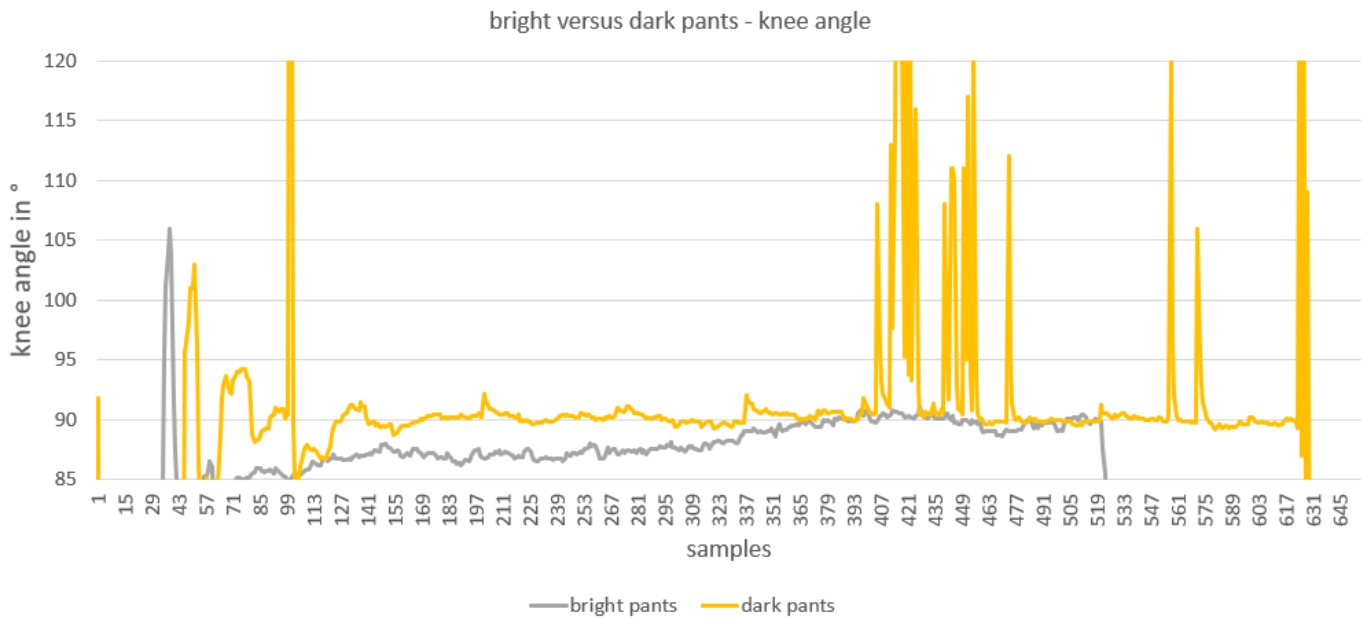


Figure 34 Knee angle plot for camera sensor derived from RGB-video of seated participant wearing dark pants and bright pants



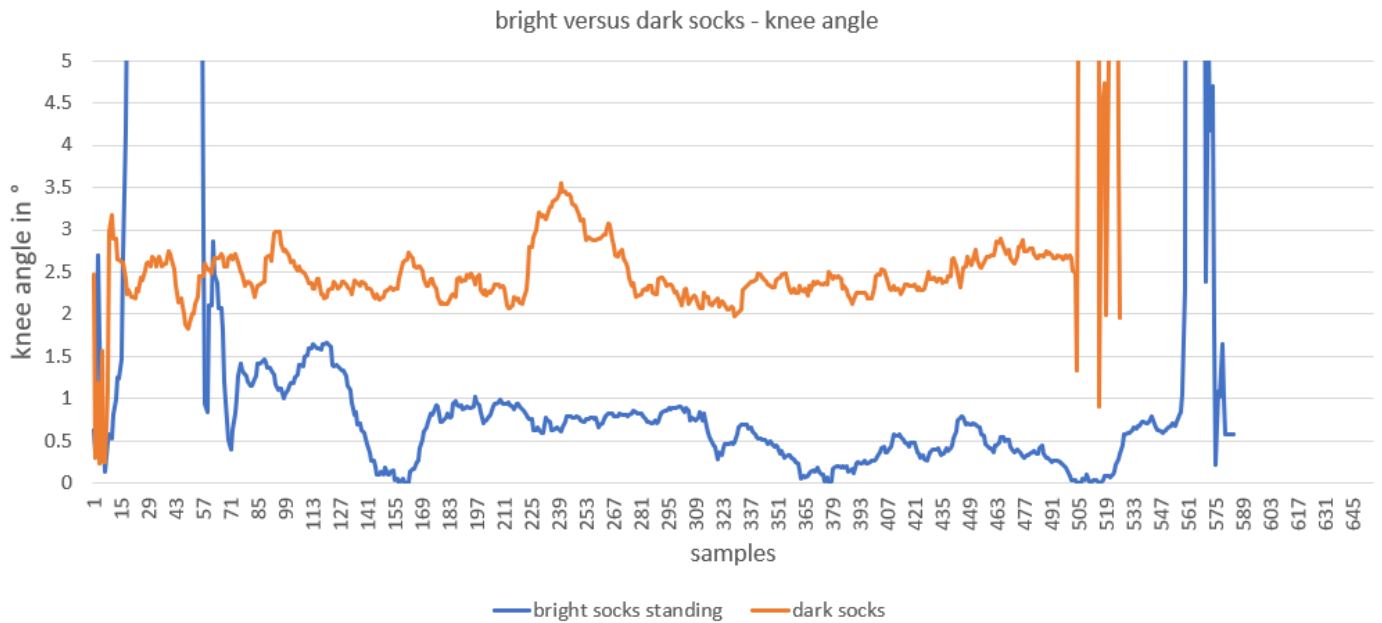


Figure 35 Knee angle plot for camera sensor derived from RGB-video of standing participant wearing dark socks and bright socks

When plotting the data of this test over time, a higher noise is prominent (Figure 34). A similar effect can be seen with a sock-background color match (Figure 33 - B). In this case, no noise was added but the average value was higher (Figure 33 - C) (bright socks 1°, dark socks 3°). When plotting the data (Figure 35), and watching the verification video a stable (low standard deviation) offset can be observed (Figure 33 - B).

### Parameter 3 – Light conditions

Table 9 Average and standard deviation for plateau-period in day, well-lit night and low-lit night for seated and standing task

	seated			standing		
	day	night-high	night-low	day	night-high	night-low
avg in °	89	87	88	1	2	3
std in °	1	0	1	0	1	1

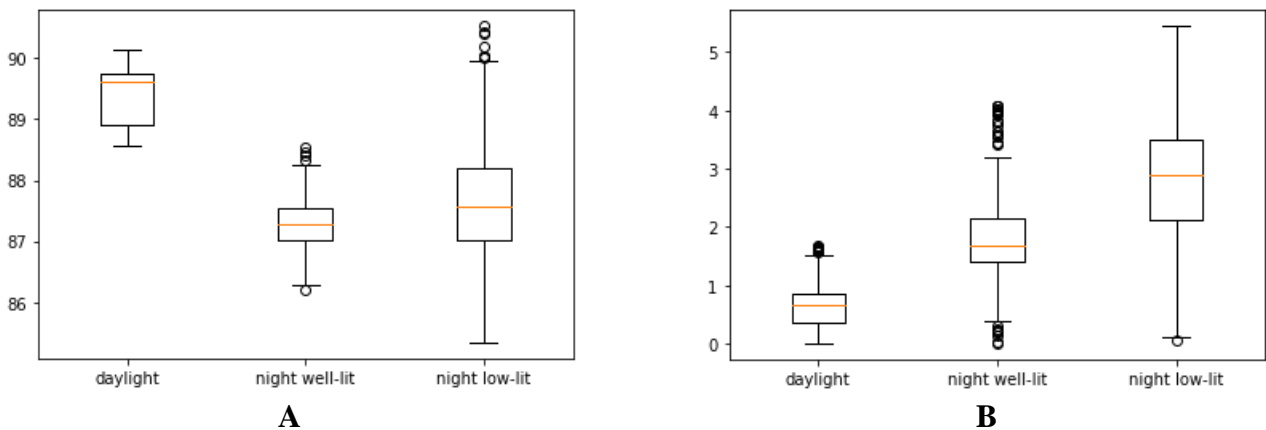


Figure 36 Boxplots of plateau-period values of seated (A) and standing (B) tasks during different light-conditions

While the boxplots show a wider spread of the datasets for the lower-light conditions (Figure 36 – A/B), the standard deviations and average measures quantify it (Table 9). In the seated task, standard deviation for day and night-low condition are equal, however the boxplot shows more outliers beyond the 25% and 75% percentile for both night-conditions (Figure 36 – A). In the seated task, both night conditions have a higher standard deviation (1° versus 0°).

## Discussion

In the beforementioned paragraphs, three tests namely offset angle, outfits and light conditions, were executed to evaluate the feasibility of the mediapipe algorithm in combination with a simple vector-based formula to detect knee angle.

In the OA-kicking test, it was seen that the smallest error for flexion was  $6^\circ$  at the predicted side-view (OA  $90^\circ$ ). The smallest error for extension was  $2^\circ$  at  $80^\circ$  OA. In the seated and standing OA-test, the smallest errors were  $1^\circ$  at  $90^\circ$  OA and  $1^\circ$  at  $80^\circ$  OA. This result confirms the hypothesis, that the suggested approach works best for a side-view ( $80^\circ$  or  $90^\circ$ ). Still, two flaws within the setup must be addressed to show its limitations. Firstly, the execution of the movement yields the disadvantage of not being able to replicate a perfect absolute value of  $0^\circ$  and  $90^\circ$ . Especially RMSE values for flexion ( $0^\circ$ ) in the kicking task might have been rather due to the variations in execution than due to the OA. Secondly, when facing the camera, a bent knee (Figure 37) would be correctly calculated as  $0^\circ$  (straight leg). This is not a flaw of the sensor, but a flaw of the mathematical foundation that derives the knee angle.

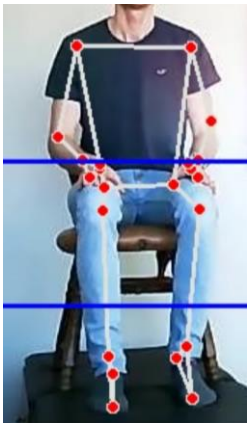


Figure 37 Front-view and detection of body landmarks in seated-bent position

Due to this fact, the ideal setup requires the patient to be placed with an OA of  $80$  to  $90^\circ$  in front of the camera. As a study tested with various angle reproduction tasks, the error of humans reproducing right angles of two connected lines was  $0.4^\circ \pm 2.6$  (50). If this implies the same for our application, we could expect both patients and physiotherapists to reach a setup with this error. Therefore, it is thought to be very unlikely that the OA would cause the accuracy requirement ( $<10^\circ$ ) to be violated.

The second test assessed the impact of different outfits. As suggested by the results, the noise increased for wearing black pants in a low-light condition. Similarly, the average over the plateau period increased for background-color matching socks. Both results can most likely be explained by a similar mechanism. As described in methods, the algorithm was optimized to always show results. For that reason, even if the confidence due to occlusion or misinterpretation is low, the hip, knee and ankle landmarks are deducted by the most confident surrounding landmarks (regression). As for the pants, it might be that the shadow creates a difficulty since it is misinterpreted as the leg. Another possibility could be the occlusion of the ankle by the pants (cuff on bottom). As for the socks, it might be that the toe landmark is fused with the background. Since the surrounding landmarks might also have a low confidence level, the toe-landmark's position can probably not be regressed accurately.

The third test evaluated the impact of light-conditions. With a higher standard deviation at low-night condition as opposed to day-lighting in both standing and seated task, the results support the hypothesis of noise introduction due to light-conditions.

Since even isolated parameters create noise (light conditions) or unpredictable deviations (outfit), combining any of the parameters is hypothesized to decrease the accuracy even more. Other parameters that could introduce additional noise or instability were not tested.

- Another person (e.g. physiotherapist) steps into the frame e.g. as he/she adjusts the movement of the patient while execution and
  - o is detected as the patient.
  - o is fused with the patient.

Since the algorithm was designed for single-person use-cases (47), this is hypothesized to be very likely.

- Occlusions are not removable between camera and patient (e.g. table, chair, plants). Although the mediapipe algorithm was optimized for accurate and quick results even on partially occluded bodies, it was not tested how much of a body needs to be visible for the well-functioning of the technology.

It could be that the algorithm performs better when the confidence-levels for detection and tracking described in the methods section are set differently. Although this comes at the cost of getting a less continuous output, these results might then be more accurate.

## Results summary and concept selection

To decide for a sensor based on the tests and considerations given in the above report, the following table provides the crucial criteria which coincide with the requirements set in the introduction phase (Table 10).

*Table 10 Crucial requirements and wishes for concept decision involving camera, IMUs and flex-sensor. The stationary spatial resolution for the camera was equal for standing and seated task. For the repetitive spatial resolution of the camera concept, the value above indicates the peak RMSE. Not tested requirements were indicated with "Nt".*

Requirements	Camera	IMUs	Flex-sensor
Temporal resolution	33 ms	6.7 ms	10 ms
Mass of sensor < 500g	0 g	52 g	20 g
Spatial resolution: Stationary, RMSE < 10°	1°	0°	1°
Spatial resolution: Repetitive movement, RMSE < 10°	6°	1°	6°
Save sensor output	Yes	Yes	Yes
<b>Wishes</b>			
Able to distinguish a squat from a CM-squat.	Nt	Nt	Nt
Workspace of knee motion: minimally 1x1x2.6m	Nt	Nt	Nt
No demand for extensive preparation (>3 min setup-time) or reclothing	No	No	Nt
relativity of system output	Yes	Yes	No
additional parameters possible (same position)	Yes	Yes	No
Quantification of CM	Nt	Nt	Nt

Concluding from the table above, all requirements were met by each sensor individually and therefore all can be deemed suitable. Wishes regarding workspace and preparation were not specifically tested. However, passing of the workspace requirement is highly probable since the spaces used in all tests are assumed to be at least of 1x1x2.6m. The preparation requirement is likely to be passed in terms of timing. However, for one of the participants, sliding of the thigh-IMU occurred after 20-25 squats. Reclothing solved this problem and thereby might be considered extensive preparation. Quantification of CM was no tested.

Although the heaviest, the IMU-system satisfies the requirement of being less than 500g. As it scores best in temporal resolution, stationary and repetitive movement spatial resolution and satisfies two wishes, it was decided to continue with this concept.

## Final design

The final design consists of hardware and software. The software part will focus on the requirement to differentiate squat and CM-squat movements. While every preconcept and the hardware part still focuses on objective 1 (knee angle acquisition), the software part focuses on objective 2 (detecting CM).

### Final Design – Hardware

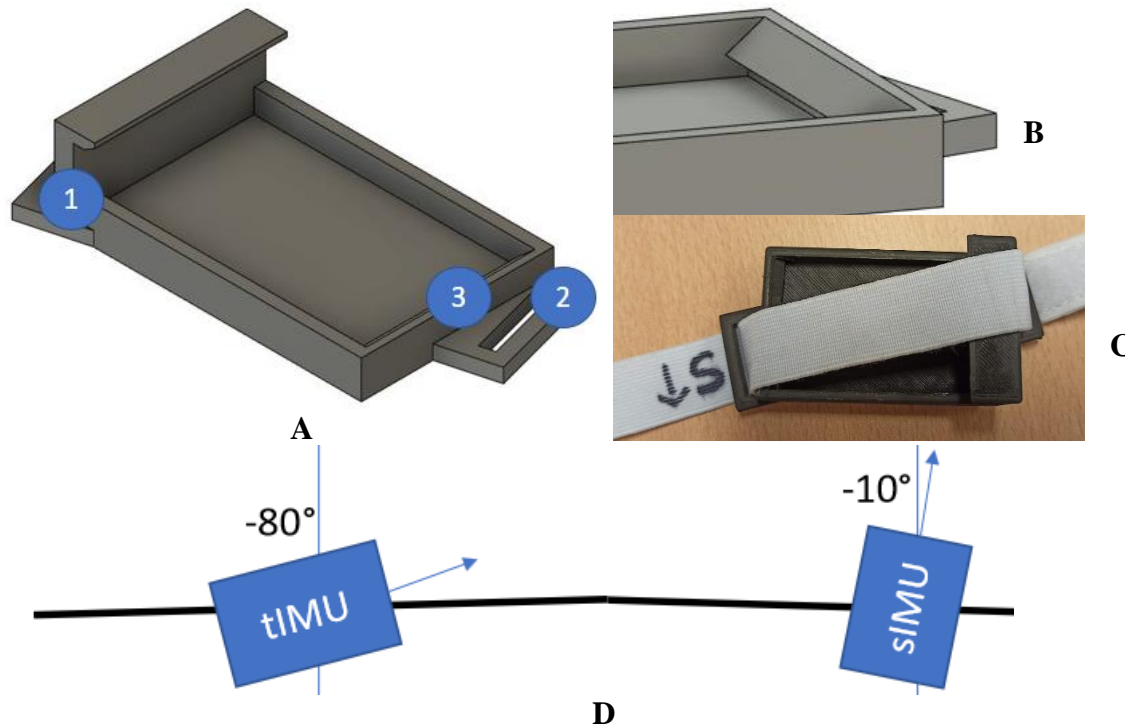


Figure 38 Schematic of casing for shank IMU with indications 1 as calibration angle, 2 as strap attachment holes and 3 as clipping mechanism (A), Close-up of area that allows for clipping mechanism (B), Printed casing with straps attached and upwards-indication (S) on left (C), Calibration angles for thigh (tIMU) and shank IMU (sIMU) (D)

The casing for each individual IMU accommodates three major features namely pre-calibration, attachment, and clipping mechanism (Figure 38).

To avoid the singularity, a calibration angle was set. Therefore, referring to the upwards-axis in a seated full-extension state and considering counter-clockwise rotation as positive, the sensor-cases were angled to  $-10^\circ$  for the shank and  $-80^\circ$  for the thigh. These angles were chosen to allow for recording of both squat and seated kicking task without falling into singularity. When thinking about it graphically (Figure 38 – A – 1, D), the arrow should never point up- or down (singularity) in neither of the ranges of motion the tasks require. To exemplify, the thigh-IMU shall be as far as possible from singularity in both extreme points. For squatting that would be standing and squatting, for the seated kicking task that is sitting with maximal flexion and extension. Since the pitch-axis has a uniquely displayable range of motion of  $180^\circ$  ( $-90^\circ$  to  $90^\circ$ ) and the requirement asks for a  $160^\circ$  range ( $-10^\circ$  to  $150^\circ$ ), I placed it in the middle.

The attachment needed to be firm, but adjustable to accommodate several patient's legs. Therefore, it was decided to use a flexible band that has Velcro-parts on the ends. These were lead through the casing's designated strap attachment holes (Figure 36 – A - 2). In order to make sure that the orientation of the system on the leg is correct, a label and an arrow indicated the correct side and direction (Figure 36 – C).

Since the sensors entailed a clip on one of the ends, the casing entails a complementary clip-holder. The ramped surface on the right (Figure 36 – A – 3, B) allows for the patient to push onto the sensor without

preloading the clip and thereby achieving a clip-in. A sharp edge on the bottom was consciously put to achieve a clicking sound once the sensor is properly attached. Taking the sensor out can be done by loading the spring and moving it up.

## Final Design - Software

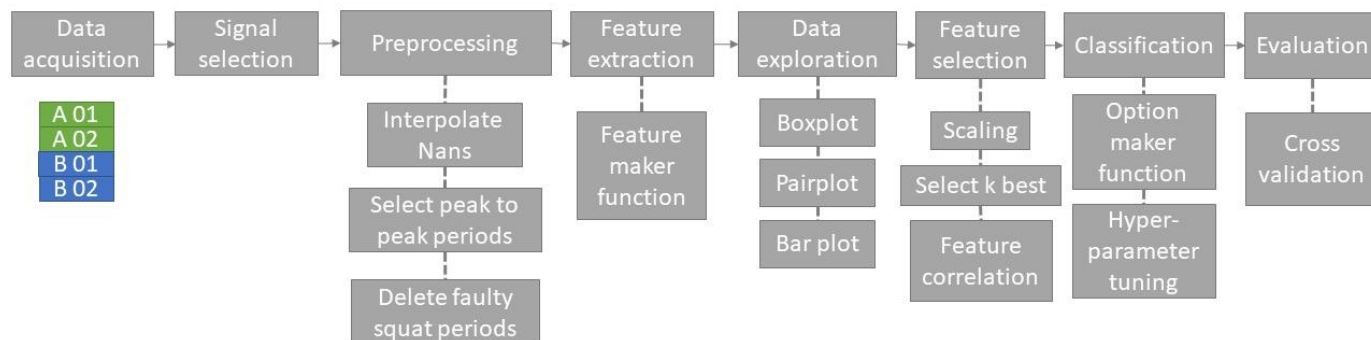


Figure 39 Flowchart describing all parts of the pipeline from original datasets to classification and evaluation. The data is passed from left to right. The first row determines steps, while the lower ones describe sub-steps within the top row's items. The datasets were named using letters for participants.

Since objective 2 identifies as detecting compensatory movements, the above pipeline was constructed to achieve that. In the following paragraphs, this classification pipeline is described for each individual step (Figure 39).

### Data acquisition

For two participants, two datasets each were recorded on two IMUs namely shank-IMU and thigh-IMU at 150 Hz. Each dataset consisted of 12-15 squat executions for ten different movement patterns (Table 11).

Table 11 Description of acquired datasets of classes in full name, short name and sentence. Within this report all texts and figures will entail the short name. Close attention needs to be paid to the labeling of "instability" since in physio-therapeutical terminology this means to be out of balance, where within this report it was used to indicate shaking of the legs.

class full name	class name short	description
full squat	fulls	Feet hip-width apart, weight on heels, flexion > 90°
half squat	halfs	Feet hip-width apart, weight on heels, flexion = 90°
x-legged squat	xlegs	Inwards rotation of legs
o-legged squat	olegs	Outwards rotation of legs
standing squat	standings	Sensor-leg raise while standing, flexion > 90°
shaking squat	instability	Shaking legs while squatting
asymmetric squat right	asymright	Asymmetrically bear weight more on right side
asymmetric squat left	asymleft	Asymmetrically bear weight more on left side
knee beyond toes squat	kneepasttoes	Heels on the floor, perpendicular of knee reaches beyond toes

### Signal selection

A series of recordings was done both on video and via the IMUs to see which signals might be the most crucial. These recordings were made with a preliminary Velcro-strap setup.

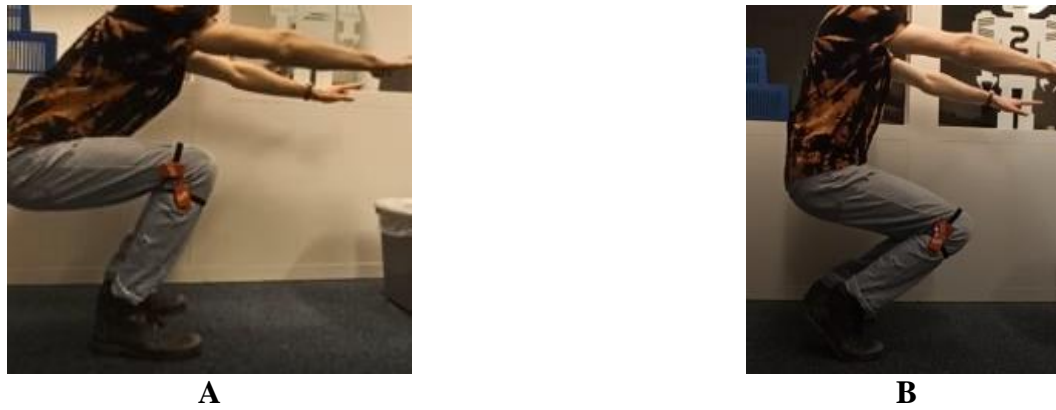


Figure 40 Participant execution of standard squat (A), heels-lift squat (B)

The video was used to get an intuitive understanding which signal might play the most detrimental role in detecting CM. As indicated in Figure 40, for the heelslift-CM, a possibly highly indicative signal was shank pitch as well as thigh pitch.

Continuing the same approach for all movements, 7 signals (roll, pitch, yaw from both IMUs and acceleration in z orientation from shank IMU) were chosen to extract features from. During these recordings, it became clear that it's hard to maintain a certain calibration angle with this setup. For that reason, a mechanical structure was developed to keep a calibration angle (for more information, see Final Design – Hardware).

## Preprocessing

### Interpolate NANs

NAN-values were identified and linearly interpolated.

### Select peak to peak periods

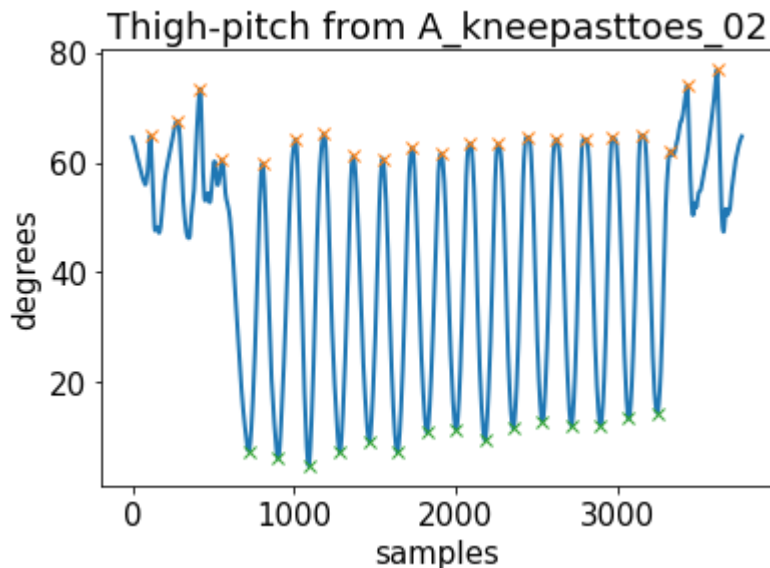


Figure 41 Degrees versus samples of participant A's second kneepasttoes recording after peak/valley detection and correction.

Each event (one squat) was isolated by utilizing the peakfinder function from the scipy library (Figure 41). The window was defined by the following properties:

- All other signals were windowed according to the indices based on thigh-pitch. This is since the thigh pitch signal was identified as an intuitive signal in terms of determining when a squat-movement is executed.

- Standing can be defined as peak, squatting as valley. This is due to the calibration angle of the thigh-IMU.
- One squat was defined as a peak-valley-peak sequence.
- Standing threshold was the mean of the overall signal.
- Squatting threshold was set as 85% of the mean of the overall signal. However, if less than twelve valleys were detected (a priori knowledge: per recording at least 12 squats), this threshold was moved upwards consecutively until at least 12 valleys were identified.
- A time-difference threshold determined the minimum sample number in between two consecutive peaks. This number was chosen due to this assumption: 150 samples / second \* 1 seconds / squat= 150 samples/squat. Accounting for quick participants, 100 samples were used.
- Since peaks might also resemble walking around or taking breaks, valleys were likelier to stem from squat-only behavior. Therefore, they were chosen to be the indicator of a squat.

Within these properties, a trade-off relationship between the number of peaks/valleys detected and the correctness of the latter was present. I.e., if every peak/valley was found, also some additional wrong ones were identified. Therefore, the window cutter thresholds were optimized to find the maximum number of peaks/valleys with the minimum number of false ones.

### Delete faulty squat-periods

If a valley was not surrounded by exactly one peak before and one after, this would be representative of either a resting period, initial/terminal period or falsely negative peak. Therefore, these squat periods were deleted.

### Feature extraction

Features were extracted from each of the windows. Features calculated were average, standard deviation, maximum, minimum, height (max – min), sum, quantiles at 25, 50 and 75%, variance, most prominent frequency in tremor spectrum and its power, slope in the first 25 and 75 samples. This was done for each individual signal (number of signals = 7), as well as the differences for all complementary signals (e.g. diff\_roll = shank-roll - thigh-roll) (number of signals = 3). Therefore, we end up with 140 features.

### Data exploration

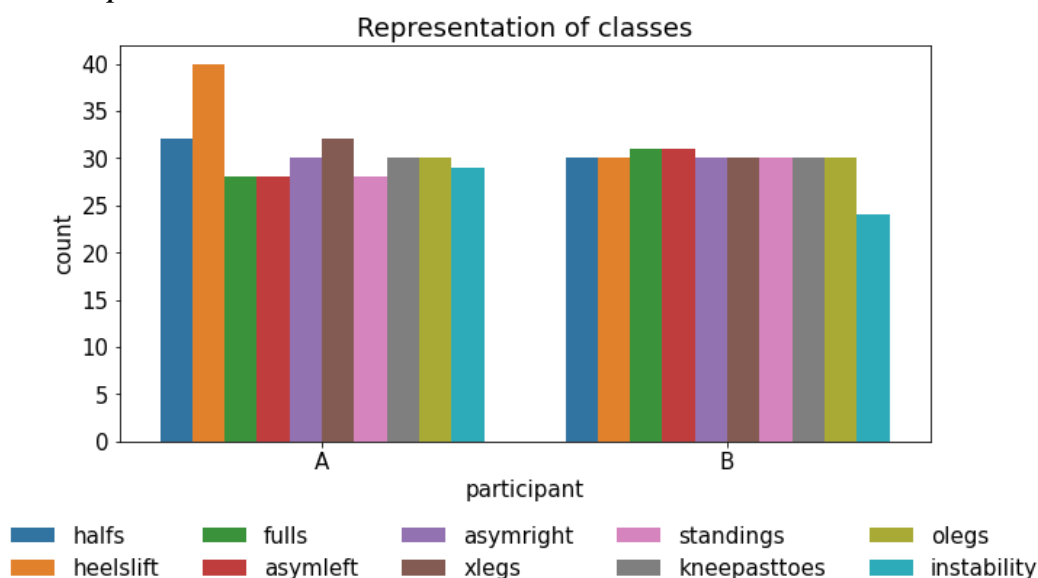


Figure 42 Barplot of all squats ordered by participants (A,B) and classes. This was done to see if there is a class-imbalance.

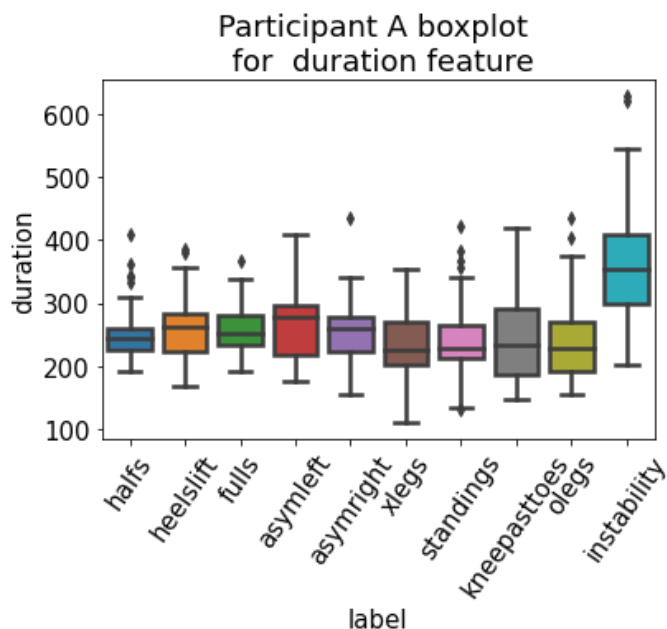


Figure 43 Boxplot showing duration feature across dataset 1 of participant A

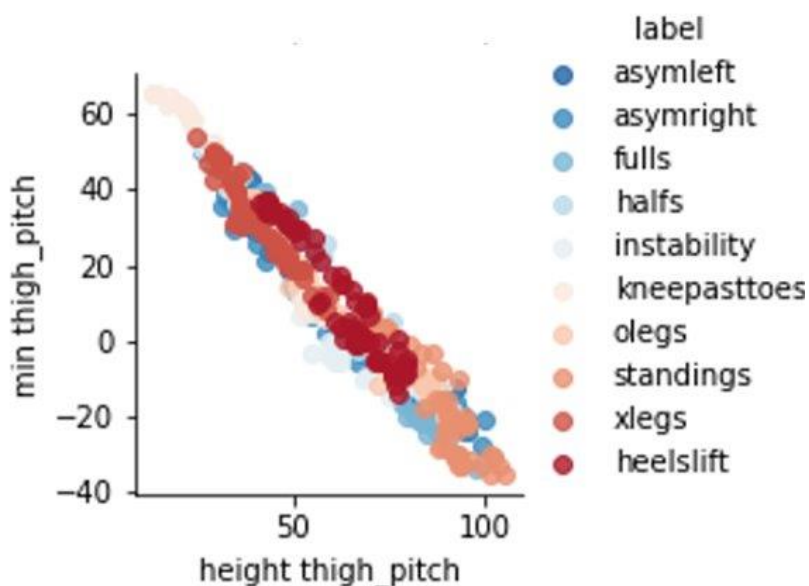


Figure 44 Pairplot of features min thigh\_pitch and height thigh\_pitch to check for feature correlation

To inspect, data exploration was done via three plots. A bar-plot was used to check for class-imbalance (Figure 42). A box-plot was used to intuitively see if there are differences between the classes for each feature (Figure 43). Lastly, a pairplot was used to see if the features correlate (Figure 44).

### Feature scaling

Each feature needs to be scaled to a unified range such that no numerically higher feature dominates the other. For that reason, it was decided to choose the MinMaxScaler from sklearn to rescale the data from 0 to 1 as recommended by (51).

### Feature Selection

In order to select the best features, the function selectkbest from the sklearn library was used. The best features were extracted with the chi-square test. This test gives an indication of how dependent target and feature variable are (52).



$$\chi_c^2 = \frac{\sum(O_i - E_i)^2}{E_i} \text{ From (34)}$$

The chi-square-test entails observed (O) and expected values (E) (Equation 14) and is used in statistics to assess the independence of two events. In feature selection, these two events are feature and class. Therefore, individual scores per feature can be calculated. If the score is high, the null-hypothesis of the chi-square-test can be rejected, i.e. class and feature are dependent and we should include the feature within our model training. While this measure excludes features that are not indicative for the class, it does not exclude highly correlated features.

Highly correlated features might cause individual decisions to yield the same classification. In e.g. the random forest classifier (explained next chapter), two decision trees with correlated features will be aggregated to have a higher voting power although the features could have been summarized as one. This causes overfitting since the model would perform well on the training dataset but fails to generalize (53).

Therefore, the pair plot was used to intuitively analyze if correlating features are present. These pairs were identified via the correlation function `corr()` and a threshold of 0.8. Then, each feature's corresponding score of the chi-square test (select k best) was crucial for keeping either. All following measures were taken in regard to this new dataset, namely one that has run through select k best and the feature correlation pipeline.

## Classification

This chapter describes the pathway from a matrix entailing features to a classification decision.

Three models were selected as for the requirement of being capable to perform multi-class, supervised classification: k-nearest neighbor (KNN), random forest classification (RFC), and support vector machine classifier (SVC). These were chosen since they were successfully used in other human activity distinguishing tasks for multi-class problems (54)(55)(56). A brief description of each of the classifiers follows.

### K-nearest neighbor

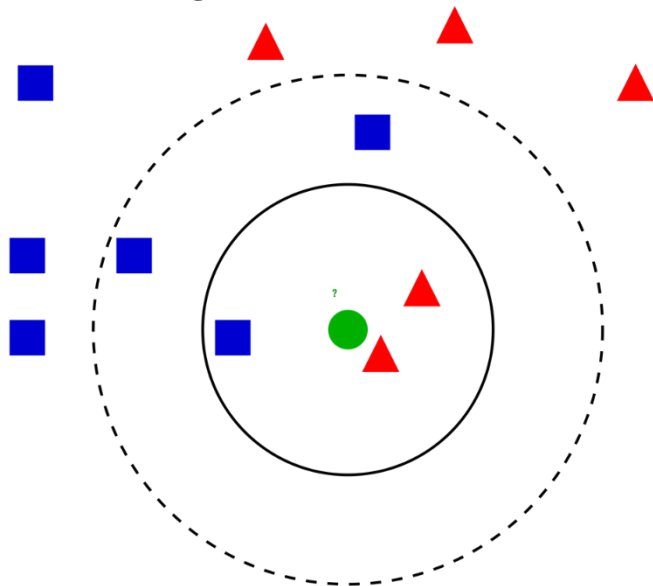


Figure 45 Intuitive graphical explanation of mechanism of K nearest neighbor. The dashed circle produces another classification (blue) than the solid line (red). From (57)

When plotting each training datapoint in an n-feature space (example for two features) (Figure 45), the KNN-algorithm finds the closest neighbors and decides the label of an unknown point based on the majority class of neighbors. A hyperparameter for this algorithm is the number of neighbors considered.

## Random Forest

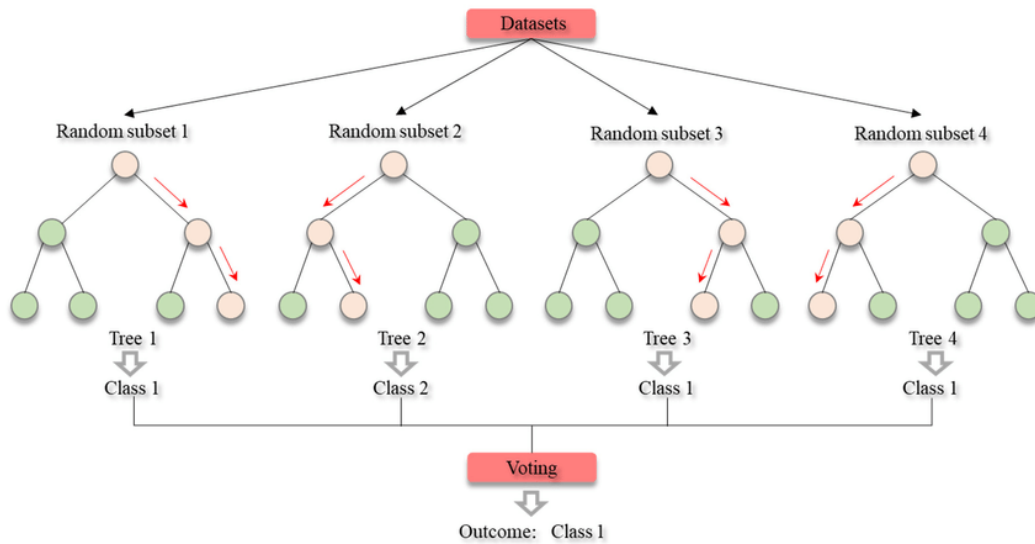


Figure 46 Intuitive graphical display of mechanism of RFC, showing individual decision trees and their aggregated decisions. From (58)

The RFC algorithm is based on the decision tree. A decision tree takes all data and forms bifurcations based on features (e.g.  $> 1$  or “entails digit 2”). Although highly intuitive, decision trees are prone to overfit since they take one line of decisions to classify an event. Therefore, RFC was developed as a collection of decision trees that each take an individual classification decision based on both a random subset of the training data (bootstrapping) and random features (Figure 46). Then, class decisions are aggregated to come up with a more robust, final decision.

Tuned hyperparameters for this algorithm are the number of trees (estimators) and the maximum number of features used per tree. These were chosen since the other parameters did not cause a change in accuracy.

## Support Vector Machine

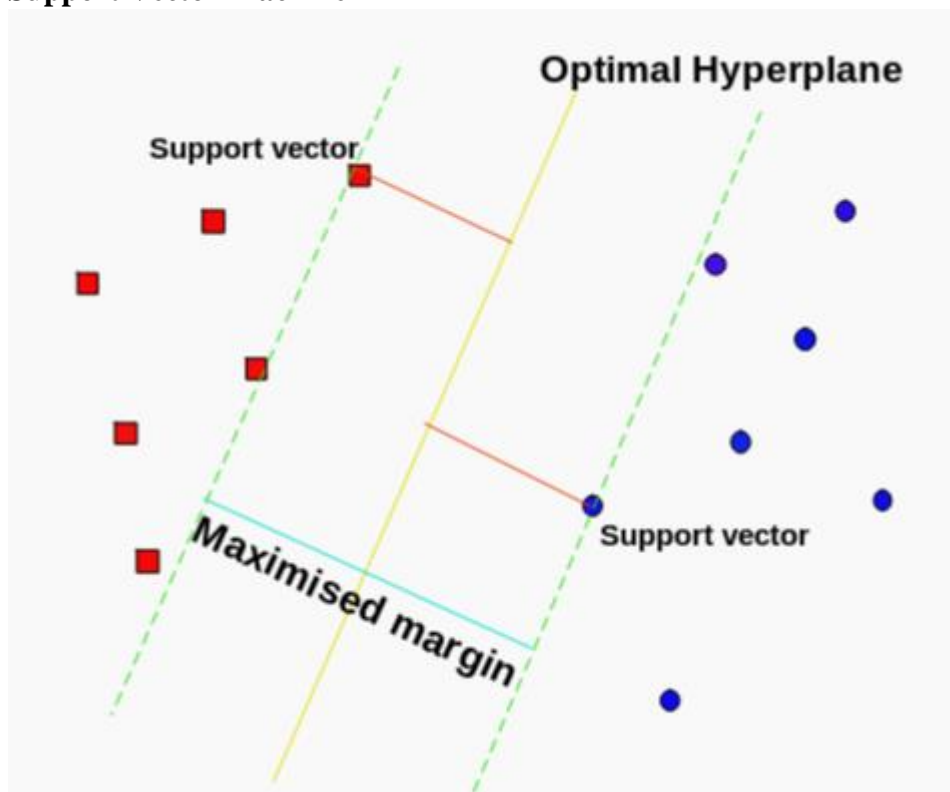


Figure 47 Intuitive graphical display of mechanism of SVC. Separator hyperplanes (lines) are used to determine class affiliation. While the yellow line leads to a more robust differentiation, the green line might cause overfitting. From (59)

Although the SVC algorithm works on the same n-feature dimension base as KNN, it forms a class decision by drawing a line or another geometrical shape (kernel) to separate the classes (Figure 47). It does so by adding another dimension with the designated kernel. The ideal hyperplane is thereby defined by the one with maximized margin. That means, it tries to increase the distance between the drawn hyperplane and any point. Hyperparameters for this algorithm are C and gamma. C determines how strictly the separation is executed. If C is high, most samples from one class will be separated from the other. This reduces generalizability but ensures most datapoints in the training set to be detected correctly. Gamma determines the reach of the support vectors, namely if datapoints further away from the decision boundary are considered.

### Classification options

This paragraph describes how the datasets can be used for two use-cases (Figure 48).

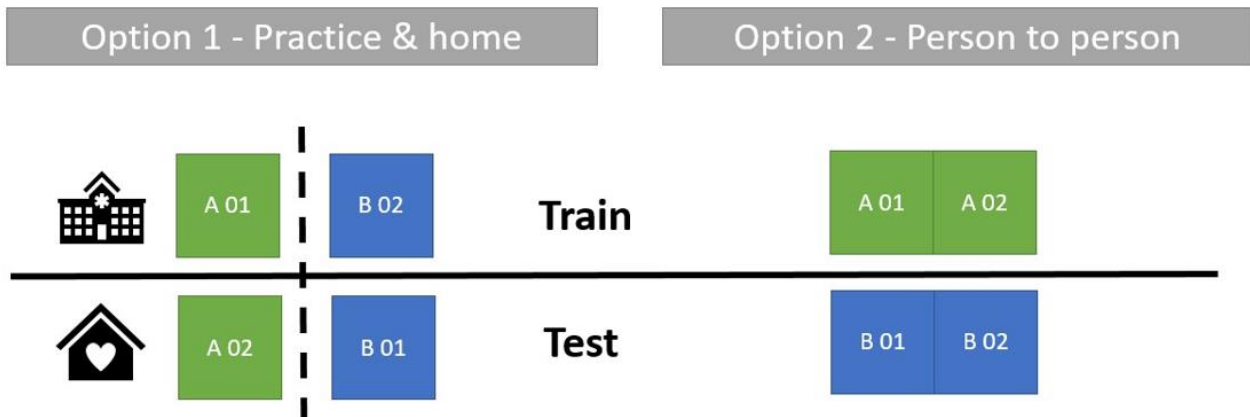


Figure 48 Options of using the datasets. Option 1 is patient-dependent and option 2 is patient-independent. Letters A and B indicate participants, while the numbers 01 and 02 indicate the datasets.

The first option describes the use-case in which the physiotherapist creates a training set per person and creates a model, after which the patient can use this model at home. The second option assesses whether the approach can be used to collect data on one patient and generalize it onto another. Potentially, this could be used in a shared-data network entailing patient information from several practices to allow for different specifications e.g. different tasks or impairments.

## Hyperparameter tuning

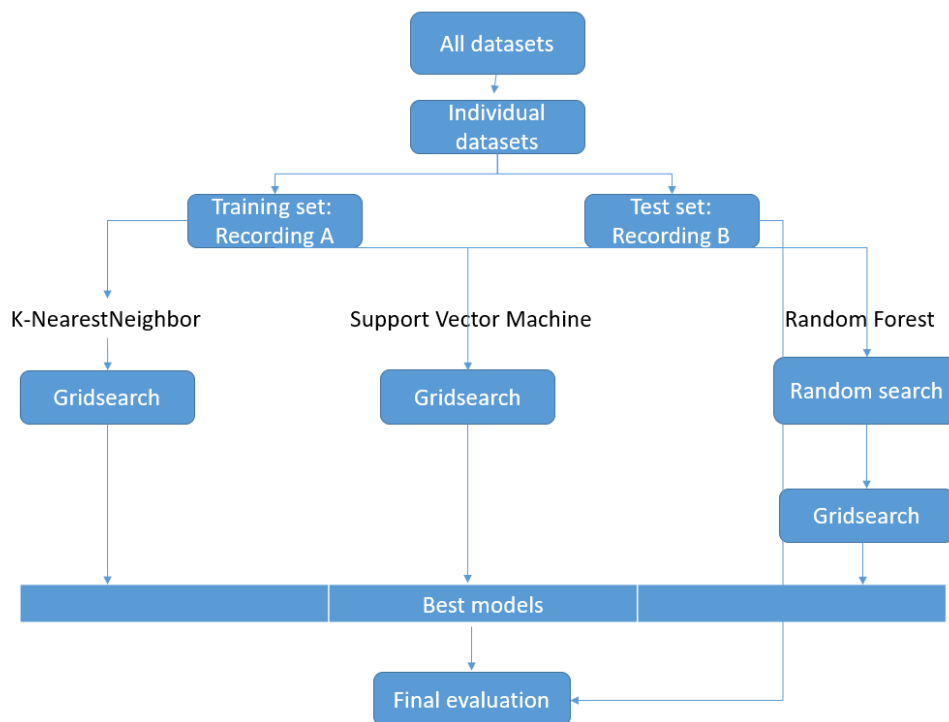


Figure 49 Hyperparameter tuning pipeline entailing three machine learning algorithms namely KNN, RFC and SVC, subsequent hyperparameter searches (grid search and random search), and final evaluation. Consider that this is an explanatory pipeline for option 2. Option 1 was executed the same way but with patient-dependent datasets 01 and 02 from both participants.

Each machine learning algorithm has certain parameters that can be tweaked to optimize it for a specific problem (hyperparameters) (Figure 49). Each dataset (Option 1 - A, Option 1 - B, Option 2) was split into test and training set to allow for later verification as described before.

Each dataset and algorithm ran through an individualized search for hyperparameters by the randomsearch (RFC) and gridsearch (all) functions from sklearn. They find the best set of hyperparameters by testing through input grids and cross-validate (three per set of parameters) with subsets of the training data to decrease the risk of overfitting. Both searches are systematically changing the hyperparameters in a different way. Randomsearch receives a grid of possible hyperparameters and randomly chooses some, whereas gridsearch runs through all possible combinations. By cross-validating each combination of hyperparameters, they make sure to not lose generalizability.

The chosen grids for random-search can be seen in the table below and were based on recommendations from current research, internet references as well as reasonability (Table 12).

Table 12 Grids for random grid-search / random-search for Random Forest Classifier (RFC), Support Vector Machine (SVC) and K-Nearest Neighbor (KNN)

RFC	start	end	SVC	start	end	KNN	start	end
estimators	5	1000	kernel	linear', 'poly', 'rbf', 'sigmoid'		n_neighbors	2	10
max features	1	X_train.shape[1]	C	2 <sup>(-3)</sup>	2 <sup>6</sup>			
			gamma	2 <sup>(-13)</sup>	2 <sup>3</sup>			

For RFC, to find a trade-off between timing and optimization, two parameters were optimized (n\_estimators and max\_features), while other parameters stayed in default-state (60). SVC ranges were chosen due to (61)(51). K-nearest neighbors were chosen to be robust (>1), and an end-range was chosen that is substantially less than the amount of datapoints per class in the training set (<15). For RFC a following grid-search on the 10 values surrounding each best parameter was conducted.

Hyperparameter tuning was performed on the training subset of each individual dataset namely option 1 - dataset A, option 1 - dataset B and option 2. The scoring parameter chosen was accuracy-score and Matthew correlation coefficient due to the following reasoning.

A false positive could mean that a squat is detected, but it is a compensatory movement. Therefore, the player would be encouraged to continue the latter, thereby opposing the initial project's idea. Therefore, this is important to reduce (optimize for recall). A false negative could mean that a squat is detected as a non-squat. That would mean that the game gives the player the indication, that his movement is wrong though it is correct. This motivates the player to continue a wrong movement or discourages him to continue the game since the perfect execution the physician taught is not detected as such. It is therefore important to reduce (optimize for precision). Thus, both measures are useful to optimize for to find a trade-off between an increase in game motivation and reduction in execution error. For balanced datasets, a metric that accounts for both is accuracy. Additionally, in case the slight class-imbalance is giving overly optimistic accuracy-scores, Matthew correlation coefficient was used since it was found to be more robust as a performance metric in cases of class imbalance (62). For comparability with other studies, more commonly used metrics such as F1-score, precision, and recall were reported.

Two different classifications were done with the datasets provided. One on all labels (10) and one on two labels (squat, non-squat). For the latter case, the dataset was turned into a two-label problem by differentiating squat (fulls, halves) and non-squat (all other labels).

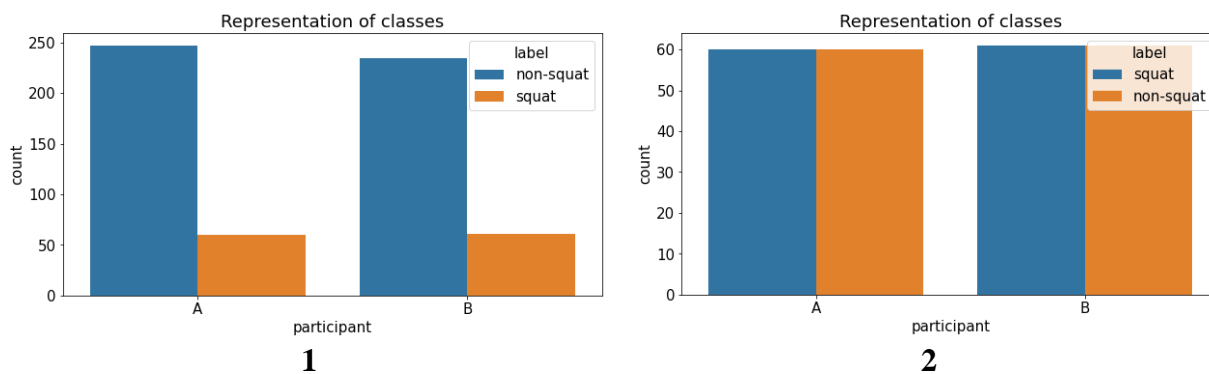


Figure 50 Barplots of class-distributions. Initial class imbalance after relabeling (1), adjusted class-balance after downsampling (2)

After relabeling, a moderate class-imbalance was present (Figure 50 - 1)(63). The majority-class (non-squat) took up 79% (dataset A) and 80% (dataset B). Therefore, four random samples out of the eight non-squat classes each were drawn (32), trying to equalize the number of squats (30) (Figure 50 - 2).

For these two options we could state two hypotheses.

1. We hypothesize to be able to distinguish 10 different squat movements (including CM and normal squatting) via machine learning with an accuracy of more than 70%.
2. We hypothesize to be able to distinguish normal squatting from squatting with CM via machine learning with an accuracy of more than 70%.

# Results

Table 13 Results for 10- and 2-label classification problem shown as accuracy, f1-score, Matthew correlation coefficient, precision and recall for each dataset namely option 1 A, option 1 B, option 2. If the best score was achieved by a hyperparameter-tuned model, it is indicated by a leading "best\_".

dataset	model	features	accuracy	matcorcoef	f1	precision	recall	labels
option 1 - A	base_SVC	9	0,52	0,50	0,47	0,47	0,52	10
option 1 - B	base_KNN	9	0,47	0,43	0,38	0,37	0,47	10
option 2	base_SVC	35	0,45	0,41	0,38	0,53	0,45	10
option 1 - A	best_RFC	9	0,75	0,53	0,79	0,68	0,94	2
option 1 - B	best_RFC	9	0,89	0,80	0,88	1,00	0,78	2
option 2	best_RFC	2	0,94	0,89	0,94	1,00	0,89	2

Judging from (Table 13), hypothesis 1 must be falsified for any of the options. Hypothesis 2 cannot be falsified for all datasets.

## Ten labels – Confusion matrices

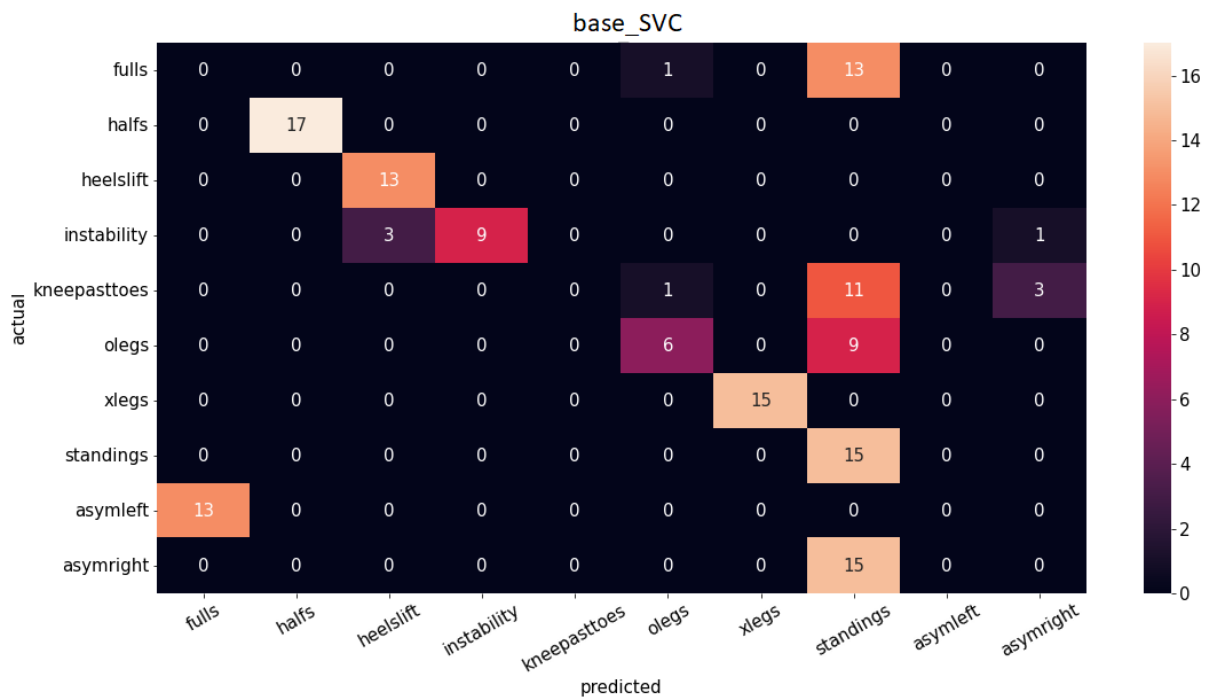


Figure 51 Option 1 – participant A – Confusion matrix for 10 labels classification

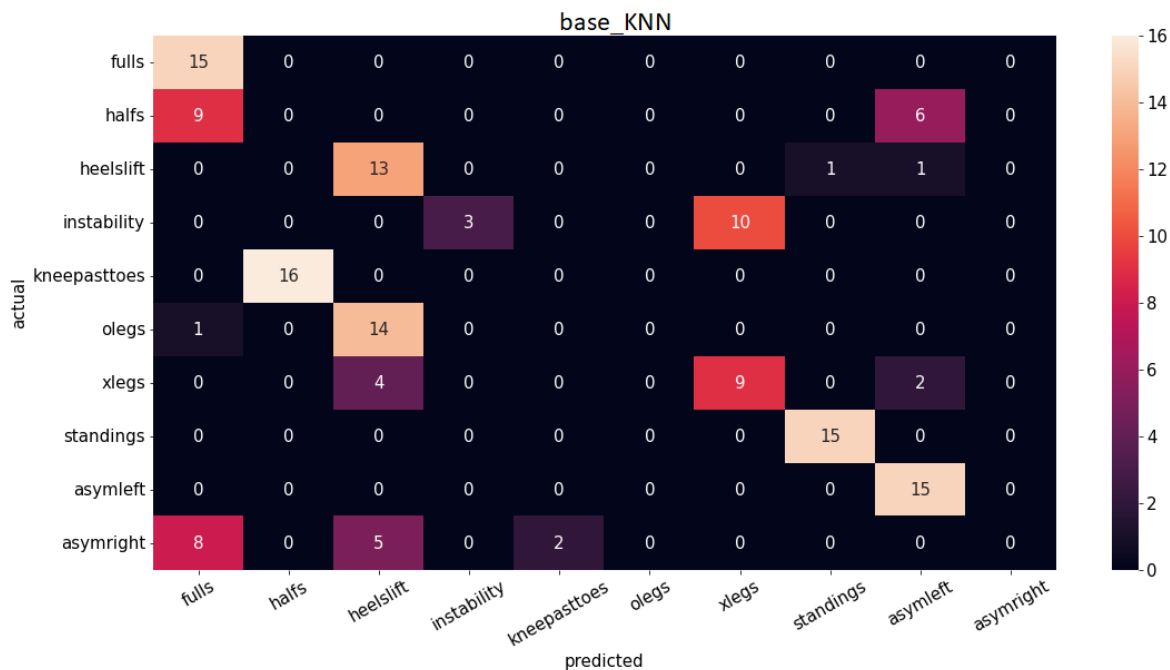


Figure 52 Option 1 – participant B – Confusion matrix for 10 labels classification

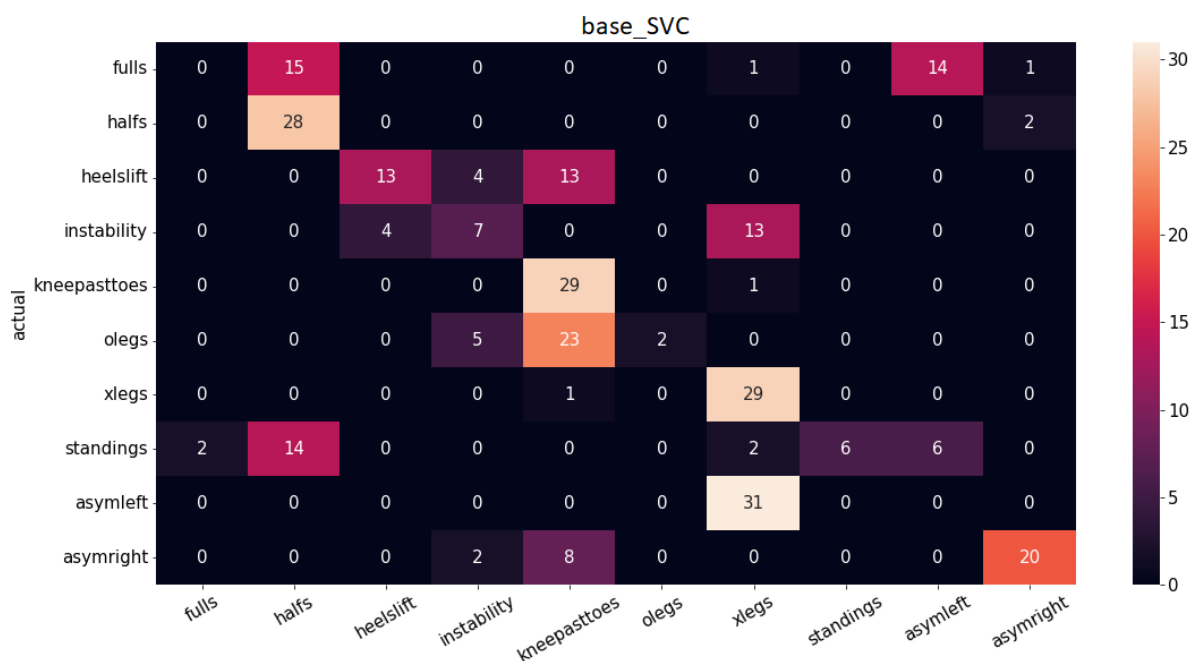


Figure 53 Option 2 – Confusion matrix for 10 labels classification

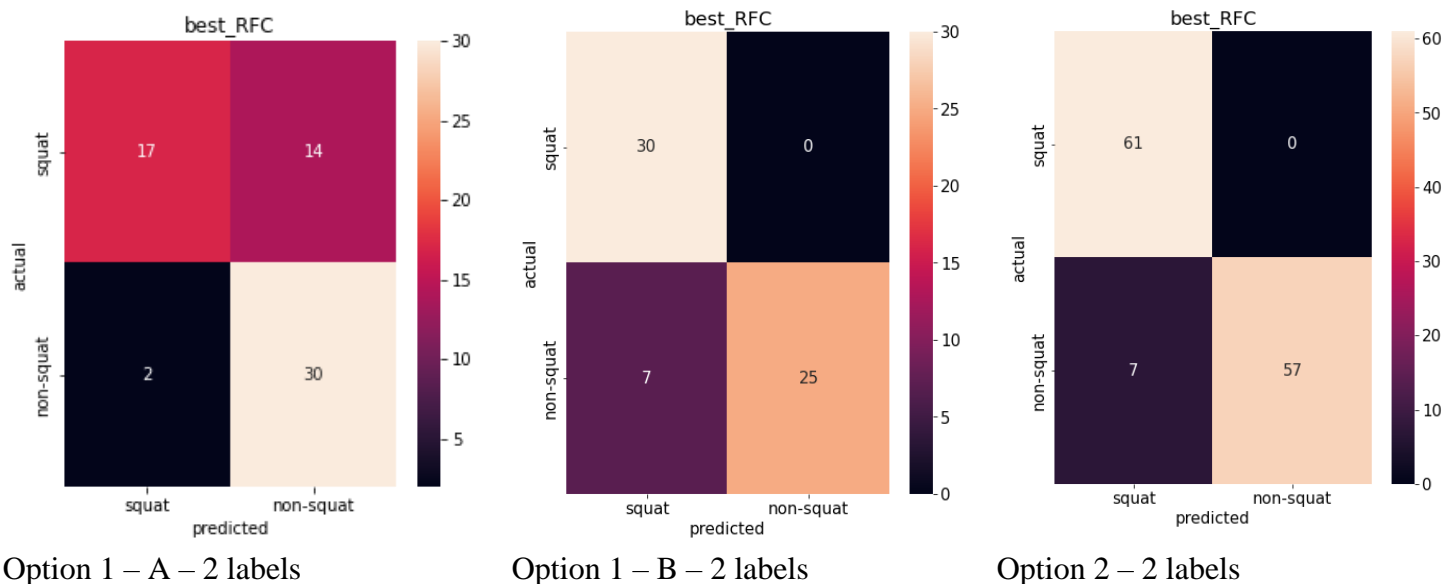
The best model for Option 1 – dataset A is base\_SVC with an accuracy of 52% (Table 13). The algorithm was able to detect labels ‘xlegs’ and ‘standings’ best, while labels ‘fulls’, ‘kneepastoes’, ‘olegs’, ‘asymleft’ and ‘asymright’ were never correctly detected (Figure 51).

The best model for Option 1 – dataset B is base\_KNN with an accuracy of 47% (Table 13). While it detected fulls, standings and asymleft with a maximum true positive rating, halves, kneepastoes, olegs, and asymright were never detected correctly (Figure 52).

The best model for Option 2 is base\_SVC with an accuracy of 45% (Table 13). While halves were always correctly detected, fulls and asymleft were never detected correctly (Figure 53).

For the ten-label classification, none of the hyperparameter-tuned models showed increased performance (Table 13).

## Two labels



Option 1 – A – 2 labels

Option 1 – B – 2 labels

Option 2 – 2 labels

Figure 54 Confusion matrices after two-label classification problem for option 1 participant A, B and option 2

For the binary classification task, the tuned RFC scored best with accuracies of 75% for dataset A, 89% for dataset B and 94% for option 2. In all datasets, hyperparameter tuning was successful in the pursuit of increasing performance (Table 13).

While in dataset A, the algorithm caused more squats to be detected as non-squats (14 vs. 0), dataset B detected more non-squats as squats (7 vs. 14) (Figure 54). In the second option, the algorithm detected 7 non-squats as squats (Figure 54).



## Discussion

Due to the nature of the design, the camera-sensor was the only pre-concept that was tested on human body data and not with a test-stand as for the flex-sensor and IMUs. Therefore, it is to be questioned if the IMU would still be superior if all concepts were tested in a human body setting.

Another project showed (45), that one main difficulty to acquire knee angle with the Xsens sensors was to avoid singularity without the need for calibrating an entire set of 17 IMUs. This thesis used a casing that entails a calibration angle to allow for full range of motion ( $-10^{\circ}$  to  $150^{\circ}$ ) recordings for the squat and seated kicking task with two IMUs only. This increase in usability is desired for a home-setting. At the same time, the MATLAB-code that allows for this recording is not designed in a user-friendly way and can only be executed by running MATLAB. A future project could expand this approach and connect the code to a graphical user interface.

Two indicators can be mentioned why there seems to be no (sufficient) generalizability from the training to the test datasets in the ten-label case. The first indicator is the accuracy which is highest for dataset A with the base\_SVC classifier (52%) and for dataset B with the base\_KNN classifier (47%). The second indicator is the unsuccessful hyperparameter tuning on both datasets for Option 1 (no “best\_” in Table 10). That shows that optimizing the training dataset’s feature contribution and decision arrangement (hyperparameter tuning) does not project onto the test dataset. I.e. the test datasets seem to be too different for a trained model to give a sufficient judgement. This might be due to the fact, that the datasets were recorded, assuming that giving a simple oral explanation will give 10 different, isolated squat-varieties. However, movement execution of one type might be fused with the other. Also, it was thought that the datasets recorded for this thesis were unlikely to produce results achieving objective 2 (in the ten-label case) which was the case as shown by the accuracy for option 2 with the base\_SVC classifier (45%). This might be due to the fact that the number of participants was small (2) and their body structure was different. Since relabeling to simplify the classification problem was possible, this particular parameter was checked for improvement. It is to be answered if any other parameters (e.g. using more participants, more features, more sensors) has a crucial impact. Although some features were created using squat-specific knowledge (slope and tremor frequency features), another possible limitation might be that the features were not tailored to the purpose. Zhang et al. (2014) tried to distinguish non-CM gait from CM gait due to lower-limb fatigue (64). Seventeen individuals participated and kinematic, time and frequency information were derived from IMU-data from shank and sternum. Intra-participant accuracy was 97% (this project 75% for A and 89% for B), inter-subject accuracy was 88% (this project 94%). They included features such as resultant acceleration, skewness, kurtosis, and resultant jerk. Adding these to the feature extraction of our dataset might improve accuracy. On the one hand, the score for inter-subject accuracy is higher in this project, and therefore must be seen with caution since it shall be tested if the generalizability of option 2 expands beyond two participants. On the other hand, these findings were surprising and infer that a system that entails several databases from independent practices could work. Adding to this, it needs to be emphasized that the datasets were recorded with two healthy participants. For that reason, it is to be questioned if a generalization of this approach to patients is possible since their capabilities of reproducing a specific type of squat is impaired. However, as option 2 showed in the binary use-case, it might be possible to train using a healthy dataset and then generalizing this onto a patient population.

A potential use-case for the two-label algorithm can be to have a patient perform an entire home-training session with a multitude of exercises (e.g. squatting, seated kicking task). The classification results for each exercise would indicate weaknesses in particular exercises. As preparation for the next in-practice session, the physiotherapist could examine which of the tasks yielded the worst scores and focus on these.

The proposed approach only allows for reward-based post-squat feedback. I.e. only after execution, a classification is made. This is not ideal for home-training since it requires the patient to remember prior

movements instead of receiving feedback mid-execution and adjust his/her movements accordingly. Using the same approach and datasets, it could be tested how the classification performance changes in case of e.g. 25% squat-duration. Although this might be able to pick up a classification earlier, it will only be able to catch errors within that interval. Potentially, a moving window could be used that classifies every  $x$  samples. However, this approach was thought to be unreasonable since for every window there needs to be a separate model trained. Alternatively, by giving feedback as a function of time along a predetermined pathway, trajectory-based feedback might pose a robust solution for this problem. Trajectory analysis is used in many different human movement tasks such as gait and balance analysis (65). A study testing the impact of trajectory-based feedback on a circle-drawing task showed only early-stage improvements. They implied that new tasks can be acquired well using this approach, however they hypothesized that in later motor learning stages, proprioception dominates judgement on good execution as opposed to the feedback (66). Mapping these findings onto our use-case, we could implement a reverse-order approach: first home-training for individual exercises, then in-practice training. It seems that these findings can be projected onto physio-therapeutical tasks due to the findings of another study. Basalp et al. (2019) trained naïve participants on a trunk-arm sweep rowing task in a rowing simulator with a pre-recorded expert-rower trajectory and found reduction in spatial and velocity errors (67). By calculating the RMSE between the actual and the ideal trajectory, the approach would satisfy the requirement of CM quantification.

## Conclusion

The first objective of designing a system that can acquire knee angle was achieved by a concept based on a two-IMU concept. The second objective to achieve more than 70% accuracy was not achieved for the patient-dependent and patient-independent options in the ten-labels classification problem. However, in the binary classification task, the objective was reached for both options [table all results]. Physio-therapeutic sessions that are designed for rehabilitation have a slowly progressing outcome and are highly repetitive [P]. These properties are hypothesized to make the patient lose motivation. That might not be the case for onsite sessions since the presence of the physiotherapist extrinsically motivates the patient. However, at home uses will not benefit from such a training program. Therefore, combining the given approach with a serious gaming environment might cause a synergy effect of fun and training is hypothesized to increase rehabilitation success [P]. Using similar two-label (CM, non-CM) datasets for other tasks which are recorded by healthy individuals might allow for a generalization onto a patient population as suggested by the results of this project. These tasks could entail typical physio-therapeutic movements such as seated kicking or seated shank rotation. For each of the tasks, a game could be developed that predominantly needs knee angle or shank rotation angle as an input to govern the character's response. Simultaneously, an input to the game would also be whether the movement was executed sufficiently, i.e. if a CM was present.

## References

[P]: Conversation with Hans Timmerman (Physiotherapist at UMCG, Groningen) personal on 2022/03/01, via phone on 2022/04/10 and 2022/06/10 and Lennart Kahl (Physiotherapist at Park-Klinik Manhagen, Großhansdorf Germany) via phone on 2022/02/17

1. Knee Bones: Anatomy, Function & Injuries - Knee Pain Explained [Internet]. [cited 2022 Jun 27]. Available from: <https://www.knee-pain-explained.com/kneebones.html>
2. Total Knee Replacement - OrthoInfo - AAOS [Internet]. [cited 2022 Jun 25]. Available from: <https://orthoinfo.aaos.org/en/treatment/total-knee-replacement/>
3. Martini F, Nath J, Bartholomew E. *Fundamentals in Anatomy and Physiology*. 2018;95–955.
4. Skou ST, Roos EM, Laursen MB, Rathleff MS, Arendt-Nielsen L, Simonsen O, et al. A Randomized,

- Controlled Trial of Total Knee Replacement. *N Engl J Med* [Internet]. 2015 Oct 22 [cited 2022 Jun 25];373(17):1597–606. Available from: <https://pubmed.ncbi.nlm.nih.gov/26488691/>
5. Price AJ, Alvand A, Troelsen A, Katz JN, Hooper G, Gray A, et al. Knee replacement. *Lancet* (London, England) [Internet]. 2018 Nov 3 [cited 2022 Jun 25];392(10158):1672–82. Available from: <https://pubmed.ncbi.nlm.nih.gov/30496082/>
  6. Bayliss LE, Culliford D, Monk AP, Glyn-Jones S, Prieto-Alhambra D, Judge A, et al. The effect of patient age at intervention on risk of implant revision after total replacement of the hip or knee: a population-based cohort study. *Lancet* (London, England) [Internet]. 2017 Apr 8 [cited 2022 Jun 25];389(10077):1424–30. Available from: <https://pubmed.ncbi.nlm.nih.gov/28209371/>
  7. Kerkhoffs GMMJ, Servien E, Dunn W, Dahm D, Bramer JAM, Haverkamp D. The influence of obesity on the complication rate and outcome of total knee arthroplasty: a meta-analysis and systematic literature review. *J Bone Joint Surg Am* [Internet]. 2012 Oct 17 [cited 2022 Jun 25];94(20):1839–44. Available from: <https://pubmed.ncbi.nlm.nih.gov/23079875/>
  8. Kurtz T, Smith J, Röder C, Ong L, Widmer R, et al. International Survey of Primary and Revision Total Knee Replacement. [cited 2022 Jun 30]; Available from: <http://www.eucomed.be/>
  9. Pinedo-Villanueva R, Khalid S, Wylde V, Gooberman-Hill R, Soni A, Judge A. Identifying individuals with chronic pain after knee replacement: A population-cohort, cluster-analysis of Oxford knee scores in 128,145 patients from the English National Health Service 11 Medical and Health Sciences 1103 Clinical Sciences. *BMC Musculoskelet Disord* [Internet]. 2018 Oct 2 [cited 2022 Jun 10];19(1):1–9. Available from: <https://bmcmusculoskeletdisord.biomedcentral.com/articles/10.1186/s12891-018-2270-9>
  10. Ageberg E, Link A, Roos EM. Feasibility of neuromuscular training in patients with severe hip or knee OA: The individualized goal-based NEMEX-TJR training program. *BMC Musculoskelet Disord* [Internet]. 2010 Jun 17 [cited 2022 Jun 27];11(1):1–7. Available from: <https://link.springer.com/articles/10.1186/1471-2474-11-126>
  11. Gaffney BM, Harris MD, Davidson BS, Stevens-Lapsley JE, Christiansen CL, Shelburne KB. Multi-joint Compensatory Effects of Unilateral Total Knee Arthroplasty during High-Demand Tasks. *Ann Biomed Eng* [Internet]. 2016 Aug 1 [cited 2022 Jun 25];44(8):2529. Available from: </pmc/articles/PMC4907879/>
  12. McClelland JA, Webster KE, Feller JA. Gait analysis of patients following total knee replacement: a systematic review. *Knee* [Internet]. 2007 Aug [cited 2022 Jun 25];14(4):253–63. Available from: <https://pubmed.ncbi.nlm.nih.gov/17531493/>
  13. Pain LM, Baker R, Richardson D, Agur AMR. Effect of trunk-restraint training on function and compensatory trunk, shoulder and elbow patterns during post-stroke reach: a systematic review. <https://doi.org/10.3109/096382882014932450> [Internet]. 2015 Apr 1 [cited 2022 Jun 25];37(7):553–62. Available from: <https://www.tandfonline.com/doi/abs/10.3109/09638288.2014.932450>
  14. Mizner RL, Snyder-Mackler L. Altered loading during walking and sit-to-stand is affected by quadriceps weakness after total knee arthroplasty. *J Orthop Res* [Internet]. 2005 Sep [cited 2022 Jun 25];23(5):1083–90. Available from: <https://pubmed.ncbi.nlm.nih.gov/16140191/>
  15. Stevens-Lapsley JE, Balter JE, Kohrt WM, Eckhoff DG. Quadriceps and hamstrings muscle dysfunction after total knee arthroplasty. *Clin Orthop Relat Res* [Internet]. 2010 [cited 2022 Jun 25];468(9):2460–8. Available from: <https://pubmed.ncbi.nlm.nih.gov/20087703/>
  16. Roby-Brami A, Feydy A, Combeaud M, Biryukova E V., Bussel B, Levin MF. Motor compensation and recovery for reaching in stroke patients. *Acta Neurol Scand* [Internet]. 2003 May 1 [cited 2022 Jun 25];107(5):369–81. Available from: <https://onlinelibrary.wiley.com/doi/full/10.1034/j.1600-0404.2003.00021.x>

17. Hamacher D, Bertram D, Fölsch C, Schega L. Evaluation of a visual feedback system in gait retraining: A pilot study. *Gait Posture*. 2012 Jun 1;36(2):182–6.
18. Lamplot JD, Bansal A, Nguyen JT, Brophy RH. Risk of Subsequent Joint Arthroplasty in Contralateral or Different Joint After Index Shoulder, Hip, or Knee Arthroplasty: Association with Index Joint, Demographics, and Patient-Specific Factors. *J Bone Joint Surg Am* [Internet]. 2018 Oct 10 [cited 2022 Jun 28];100(20):1750. Available from: [/pmc/articles/PMC6636793/](https://pubmed.ncbi.nlm.nih.gov/30387528/)
19. Xiao B, Chen L, Zhang X, Li Z, Liu X, Wu X, et al. Design of a virtual reality rehabilitation system for upper limbs that inhibits compensatory movement. *Med Nov Technol Devices*. 2022 Mar 1;13:100110.
20. Knee Range Of Motion: How To Measure & Improve - Knee Pain Explained [Internet]. [cited 2022 Jun 25]. Available from: <https://www.knee-pain-explained.com/knee-range-of-motion.html>
21. Christiansen CL, Bade MJ, Davidson BS, Dayton MR, Stevens-Lapsley JE. Effects of weight-bearing biofeedback training on functional movement patterns following total knee arthroplasty: A randomized controlled trial. *J Orthop Sports Phys Ther* [Internet]. 2015 Sep 1 [cited 2022 Jun 28];45(9):647–55. Available from: <https://www.jospt.org/doi/10.2519/jospt.2015.5593>
22. Zeni J, Abujaber S, Flowers P, Pozzi F, Snyder-Mackler L. Biofeedback to promote movement symmetry after total knee arthroplasty: A feasibility study. *J Orthop Sports Phys Ther* [Internet]. 2013 [cited 2022 Jun 28];43(10):715–26. Available from: [www.jospt.org](http://www.jospt.org)
23. Cai S, Li G, Zhang X, Huang S, Zheng H, Ma K, et al. Detecting compensatory movements of stroke survivors using pressure distribution data and machine learning algorithms. *J Neuroeng Rehabil* [Internet]. 2019 Nov 4 [cited 2022 Jun 25];16(1):1–11. Available from: <https://jneuroengrehab.biomedcentral.com/articles/10.1186/s12984-019-0609-6>
24. Borges CM, Silva C, Salazar AJ, Silva AS, Correia M V, Santos RS, et al. COMPENSATORY MOVEMENT DETECTION THROUGH INERTIAL SENSOR POSITIONING FOR POST-STROKE REHABILITATION.
25. Zeni JA, Flowers P, Bade M, Cheuy V, Stevens-Lapsley J, Snyder-Mackler L. Stiff knee gait may increase risk of second total knee arthroplasty. *J Orthop Res* [Internet]. 2019 Feb 1 [cited 2022 Jun 25];37(2):397–402. Available from: <https://pubmed.ncbi.nlm.nih.gov/30387528/>
26. Beswick AD, Wylde V, Gooberman-Hill R, Blom A, Dieppe P. What proportion of patients report long-term pain after total hip or knee replacement for osteoarthritis? A systematic review of prospective studies in unselected patients. *BMJ Open* [Internet]. 2012 [cited 2022 Jun 25];2(1). Available from: <https://pubmed.ncbi.nlm.nih.gov/22357571/>
27. Lorenzetti S, Ostermann M, Zeidler F, Zimmer P, Jentsch L, List R, et al. How to squat? Effects of various stance widths, foot placement angles and level of experience on knee, hip and trunk motion and loading. *BMC Sports Sci Med Rehabil*. 2018;10(1).
28. Hancock GE, Hepworth T, Wembridge K. Accuracy and reliability of knee goniometry methods. *J Exp Orthop* [Internet]. 2018 Dec 1 [cited 2022 Jun 25];5(1). Available from: [/pmc/articles/PMC6195503/](https://pubmed.ncbi.nlm.nih.gov/30387528/)
29. Stauffert J-P, Niebling F, Latoschik ME. Latency and Cybersickness: Impact, Causes, and Measures. A Review. *Front Virtual Real*. 2020 Nov 26;0:31.
30. Busch A, Trounson K, Browne P, Robertson S. Effects of lower limb light-weight wearable resistance on running biomechanics. *J Biomech*. 2022 Jan 1;130:110903.
31. Yin L, Chen K, Guo L, Cheng L, Wang F, Yang L. Identifying the Functional Flexion-extension Axis of the Knee: An In-Vivo Kinematics Study. *PLoS One* [Internet]. 2015 Jun 3 [cited 2022 Jun 25];10(6). Available from: [/pmc/articles/PMC4454551/](https://pubmed.ncbi.nlm.nih.gov/26111110/)

32. Kim HY, Kim KJ, Yang DS, Jeung SW, Choi HG, Choy WS. Screw-home movement of the tibiofemoral joint during normal gait: Three-dimensional analysis. *CiOS Clin Orthop Surg*. 2015 Sep 1;7(3):303–9.
33. Kaltenborn FM, Evjenth O, Kaltenborn TB, Morgan D, Eileen Vollowitz. *Manual mobilization of the joints : the Kaltenborn method of joint examination and treatment*. 4th ed. / Oslo ;Minneapolis MN: Olaf Norlis Bokhandel ;;OTTP (Orthopedic Physical Therapy Products); 2003. 336 p.
34. Papula L. *Mathematik für Ingenieure und Naturwissenschaftler Band 1*. Math für Ingenieure und Naturwissenschaftler Band 1. 2014;
35. Corke P. *Robotics, Vision and Control - Fundamental Algorithms In MATLAB® Second, Completely Revised, Extended And Updated Edition*. *Ann Math Artif Intell* [Internet]. 2017 [cited 2022 Jun 25];75(1–2):693. Available from: <https://www.springer.com/gp/book/9783319544120>
36. Aitken SA. Normative Values for Femoral Length, Tibial Length, and the Femorotibial Ratio in Adults Using Standing Full-Length Radiography. *Osteology*. 2021 May 13;1(2):86–91.
37. Kirkley A, Mohtadi N, Ogilvie R. The effect of exercise on anterior-posterior translation of the normal knee and knees with deficient or reconstructed anterior cruciate ligaments. *Am J Sports Med* [Internet]. 2001 Aug 30 [cited 2022 Jun 25];29(3):311–4. Available from: <https://journals.sagepub.com/doi/10.1177/03635465010290031001>
38. Halliday D, Resnick R, Walker J. *Fundamentals of Physics Halliday*. Wiley. 2013;
39. Bend Labs. *Soft Angular Displacement Sensor Theory Manual* [Internet]. 2021 [cited 2022 Jun 28]. p. 2–5. Available from: [https://github.com/bendlabs/two\\_axis\\_ads](https://github.com/bendlabs/two_axis_ads)
40. *Online Protractor | Angle Measuring Tool* [Internet]. [cited 2022 Jun 25]. Available from: [https://www.ginifab.com/feeds/angle\\_measurement/](https://www.ginifab.com/feeds/angle_measurement/)
41. Cloete T, Scheffer C. Repeatability of an off-the-shelf, full body inertial motion capture system during clinical gait analysis. *Annu Int Conf IEEE Eng Med Biol Soc IEEE Eng Med Biol Soc Annu Int Conf* [Internet]. 2010 [cited 2022 Jun 25];2010:5125–8. Available from: <https://pubmed.ncbi.nlm.nih.gov/21095808/>
42. Xsens. *MTw Awinda User Manual* [Internet]. 2018 [cited 2022 Jun 25]. Available from: [https://www.xsens.com/hubfs/Downloads/Manuals/MTw\\_Awinda\\_User\\_Manual.pdf](https://www.xsens.com/hubfs/Downloads/Manuals/MTw_Awinda_User_Manual.pdf)
43. Seitz F, Zeitlhöfler J, Mathis Bloßfeld D-I. Nominal and observation-based attitude realization for precise orbit determination of the Jason satellites [Internet]. 2019 [cited 2022 Jun 25]. Available from: <https://mediatum.ub.tum.de/doc/1535899/1535899.pdf>
44. Koch V, Koch IEEE Okanagan V. *Rotations in 3D Graphics and the Gimbal Lock Presentation Road Map*. 2016;
45. *Using Inertial Measurement Units to Calculate Knee Flexion Angle - OpenSim Documentation - Global Site* [Internet]. [cited 2022 Jun 26]. Available from: <https://simtk-confluence.stanford.edu:8443/pages/viewpage.action?pageId=21006384>
46. *Software downloads* [Internet]. [cited 2022 Jun 25]. Available from: <https://www.xsens.com/software-downloads?hsCtaTracking=62e6fd16-1936-4f65-9660-f85c413320da%7C3912eea5-ec35-43d9-b6fb-e2d1be46ee71>
47. *Google AI Blog: On-device, Real-time Body Pose Tracking with MediaPipe BlazePose* [Internet]. [cited 2022 Jun 26]. Available from: <https://ai.googleblog.com/2020/08/on-device-real-time-body-pose-tracking.html>
48. Zhang R, Zhu Z, Li P, Wu R, Guo C, Huang G, et al. Exploiting Offset-guided Network for Pose Estimation and Tracking.

49. Bulat A, Tzimiropoulos G. Human pose estimation via Convolutional Part Heatmap Regression. [cited 2022 Jun 26]; Available from: <http://www.cs.nott.ac.uk/~psxab5/>
50. Gray R, Regan D. Accuracy of reproducing angles: is a right angle special? *Perception* [Internet]. 1996 [cited 2022 Jun 26];25(5):531–42. Available from: <https://pubmed.ncbi.nlm.nih.gov/8865296/>
51. Hsu C-W, Chang C-C, Lin C-J. A Practical Guide to Support Vector Classification. 2003 [cited 2022 Jun 26]; Available from: <http://www.csie.ntu.edu.tw/~cjlin>
52. Sklearn Feature Selection via Chi2 [Internet]. [cited 2022 Jun 26]. Available from: [https://scikit-learn.org/stable/modules/generated/sklearn.feature\\_selection.chi2.html#sklearn.feature\\_selection.chi2](https://scikit-learn.org/stable/modules/generated/sklearn.feature_selection.chi2.html#sklearn.feature_selection.chi2)
53. Why, How and When to apply Feature Selection | by Sudharsan Asaithambi | Towards Data Science [Internet]. [cited 2022 Jun 26]. Available from: <https://towardsdatascience.com/why-how-and-when-to-apply-feature-selection-e9c69adfabf2>
54. Dohnálek P, Gajdoš P, Peterek T, Snášel V. An Overview of Classification Techniques for Human Activity Recognition.
55. Khanal B, Rivas P, Orduz J. Human Activity Classification Using Basic Machine Learning Models. [cited 2022 Jun 26]; Available from: <https://archive.ics.uci.edu/ml/>
56. Chinimilli PT, Redkar S, Zhang W. Human activity recognition using inertial measurement units and smart shoes. *Proc Am Control Conf*. 2017 Jun 29;1462–7.
57. K Nearest Neighbor | KNN Algorithm | KNN in Python & R [Internet]. [cited 2022 Jun 26]. Available from: <https://www.analyticsvidhya.com/blog/2018/03/introduction-k-neighbours-algorithm-clustering/>
58. Yang J, Gong J, Tang W, Shen Y, Liu C, Gao J. Delineation of urban growth boundaries using a patch-based cellular automata model under multiple spatial and socio-economic scenarios. *Sustain*. 2019 Nov 1;11(21).
59. Support Vector Machines(SVM) — An Overview | by Rushikesh Pupale | Towards Data Science [Internet]. [cited 2022 Jun 26]. Available from: <https://towardsdatascience.com/https-medium-com-pupalerushikesh-svm-f4b42800e989>
60. Hyperparameter Tuning the Random Forest in Python | by Will Koehrsen | Towards Data Science [Internet]. [cited 2022 Jun 26]. Available from: <https://towardsdatascience.com/hyperparameter-tuning-the-random-forest-in-python-using-scikit-learn-28d2aa77dd74>
61. Hyperparameter Tuning for Support Vector Machines — C and Gamma Parameters | by Soner Yıldırım | Towards Data Science [Internet]. [cited 2022 Jun 26]. Available from: <https://towardsdatascience.com/hyperparameter-tuning-for-support-vector-machines-c-and-gamma-parameters-6a5097416167>
62. Chicco D, Jurman G. The advantages of the Matthews correlation coefficient (MCC) over F1 score and accuracy in binary classification evaluation. *BMC Genomics* [Internet]. 2020 Jan 2 [cited 2022 Jun 26];21(1):1–13. Available from: <https://bmcgenomics.biomedcentral.com/articles/10.1186/s12864-019-6413-7>
63. Imbalanced Data | Data Preparation and Feature Engineering for Machine Learning | Google Developers [Internet]. [cited 2022 Jun 26]. Available from: <https://developers.google.com/machine-learning/data-prep/construct/sampling-splitting/imbalanced-data>
64. Zhang J, Lockhart TE, Soangra R. Classifying Lower Extremity Muscle Fatigue during Walking using Machine Learning and Inertial Sensors. *Ann Biomed Eng* [Internet]. 2014 Mar 1 [cited 2022 Jun 28];42(3):600. Available from: </pmc/articles/PMC3943497/>
65. Blinch J, Kim Y, Chua R. Trajectory analysis of discrete goal-directed pointing movements: How

many trials are needed for reliable data? Behav Res Methods [Internet]. 2018 Oct 1 [cited 2022 Jun 26];50(5):2162–72. Available from: <https://link.springer.com/article/10.3758/s13428-017-0983-6>

66. Effect of Real-time Visual Trajectory Feedback on Upper Limb Movement Learning | Chinese Journal of Rehabilitation Theory and Practice;(12): 217-223, 2019. | WPRIM [Internet]. [cited 2022 Jun 26]. Available from: <https://pesquisa.bvsalud.org/portal/resource/pt/wpr-905103>
67. Basalp E, Marchal-Crespo L, Rauter G, Riener R, Wolf P. Rowing Simulator Modulates Water Density to Foster Motor Learning. Front Robot AI. 2019 Aug 21;6:74.